

# Arteriosclerosis, Thrombosis, and Vascular Biology

JOURNAL OF THE AMERICAN HEART ASSOCIATION



## Disturbed Flow Promotes Endothelial Senescence via a p53-Dependent Pathway

Christina M. Warboys, Amalia de Luca, Narges Amini, Le Luong, Hayley Duckles, Sarah Hsiao, Alex White, Shukti Biswas, Ramzi Khamis, Chuh K. Chong, Wai-Mun Cheung, Spencer J. Sherwin, Martin R. Bennett, Jesus Gil, Justin C. Mason, Dorian O. Haskard and Paul C. Evans

*Arterioscler Thromb Vasc Biol.* published online March 20, 2014;  
*Arteriosclerosis, Thrombosis, and Vascular Biology* is published by the American Heart Association, 7272 Greenville Avenue, Dallas, TX 75231  
Copyright © 2014 American Heart Association, Inc. All rights reserved.  
Print ISSN: 1079-5642. Online ISSN: 1524-4636

The online version of this article, along with updated information and services, is located on the World Wide Web at:

<http://atvb.ahajournals.org/content/early/2014/03/20/ATVBAHA.114.303415>

Data Supplement (unedited) at:

<http://atvb.ahajournals.org/content/suppl/2014/03/20/ATVBAHA.114.303415.DC1.html>

**Permissions:** Requests for permissions to reproduce figures, tables, or portions of articles originally published in *Arteriosclerosis, Thrombosis, and Vascular Biology* can be obtained via RightsLink, a service of the Copyright Clearance Center, not the Editorial Office. Once the online version of the published article for which permission is being requested is located, click Request Permissions in the middle column of the Web page under Services. Further information about this process is available in the [Permissions and Rights Question and Answer](#) document.

**Reprints:** Information about reprints can be found online at:  
<http://www.lww.com/reprints>

**Subscriptions:** Information about subscribing to *Arteriosclerosis, Thrombosis, and Vascular Biology* is online at:  
<http://atvb.ahajournals.org//subscriptions/>

# Original Article

## Disturbed Flow Promotes Endothelial Senescence via a p53-Dependent Pathway

Christina M. Warboys, Amalia de Luca, Narges Amini, Le Luong, Hayley Duckles, Sarah Hsiao, Alex White, Shukti Biswas, Ramzi Khamis, Chuh K. Chong, Wai-Mun Cheung, Spencer J. Sherwin, Martin R. Bennett, Jesus Gil, Justin C. Mason, Dorian O. Haskard, Paul C. Evans

**Objective**—Although atherosclerosis is associated with systemic risk factors such as age, high cholesterol, and obesity, plaque formation occurs predominately at branches and bends that are exposed to disturbed patterns of blood flow. The molecular mechanisms that link disturbed flow–generated mechanical forces with arterial injury are uncertain. To illuminate them, we investigated the effects of flow on endothelial cell (EC) senescence.

**Approach and Results**—LDLR<sup>-/-</sup> mice were exposed to a high-fat diet for 2 to 12 weeks (or to a normal chow diet as a control) before the assessment of cellular senescence in aortic ECs. En face staining revealed that senescence-associated β-galactosidase activity and p53 expression were elevated in ECs at sites of disturbed flow in response to a high-fat diet. By contrast, ECs exposed to undisturbed flow did not express senescence-associated β-galactosidase or p53. Studies of aortae from healthy pigs (aged 6 months) also revealed enhanced senescence-associated β-galactosidase staining at sites of disturbed flow. These data suggest that senescent ECs accumulate at disturbed flow sites during atherogenesis. We used in vitro flow systems to examine whether a causal relationship exists between flow and EC senescence. Exposure of cultured ECs to flow (using either an orbital shaker or a syringe-pump flow bioreactor) revealed that disturbed flow promoted EC senescence compared with static conditions, whereas undisturbed flow reduced senescence. Gene silencing studies demonstrated that disturbed flow induced EC senescence via a p53-p21 signaling pathway. Disturbed flow–induced senescent ECs exhibited reduced migration compared with nonsenescent ECs in a scratch wound closure assay, and thus may be defective for arterial repair. However, pharmacological activation of sirtuin 1 (using resveratrol or SRT1720) protected ECs from disturbed flow–induced senescence.

**Conclusions**—Disturbed flow promotes endothelial senescence via a p53-p21–dependent pathway which can be inhibited by activation of sirtuin 1. These observations support the principle that pharmacological activation of sirtuin 1 may promote cardiovascular health by suppressing EC senescence at atheroprone sites. (*Arterioscler Thromb Vasc Biol*. 2014;34:00-00.)

JOURNAL OF THE AMERICAN HEART ASSOCIATION

FIRST PROOF ONLY

Aging is a major risk factor for the development of cardiovascular disease, and age-related changes in vascular function are hypothesized to influence the progression of atherosclerosis. One of the hallmarks of aging tissues is an impaired ability to regenerate, caused by the accumulation of senescent cells. Cellular senescence is a state of irreversible growth arrest<sup>1</sup> that can be triggered via the progressive shortening of telomeres (DNA sequence repeats that protect the ends of chromosomes) with successive rounds of cell division, known as replicative senescence.<sup>2</sup> Senescence can also

be induced by a variety of cellular stresses, independently of extensive proliferation, including oxidative stress<sup>3,4</sup> and activation of oncogenes.<sup>5</sup> The signaling pathways that promote cellular senescence vary according to the initiating stimulus, cellular context, and other factors. Senescence can be induced by p16<sup>INK4A</sup> (p16) and p14<sup>ARF</sup>/p53 signaling pathways.<sup>5-8</sup> p16 inhibits cyclin-dependent kinases 2 and 4, whereas p53 induces the cyclin-dependent kinase inhibitor p21<sup>WAF1/CIP1</sup> (p21). These pathways converge because inhibition of cyclin-dependent kinases reduces phosphorylation of the retinoblastoma protein

Received on: November 1, 2012; final version accepted on: March 10, 2014.

From the British Heart Foundation Cardiovascular Science Unit, National Heart and Lung Institute (C.M.W., A.d.L., N.A., R.K., W.-M.C., J.C.M., D.O.H.), Department of Aeronautics (S.J.S.), and MRC Clinical Sciences Centre (J.G.), Imperial College London, London, United Kingdom; Departments of Cardiovascular Science (L.L., H.D., S.H., S.B., P.C.E.) and Materials Science and Engineering (A.W., C.K.C.) and Insigneo Institute of In Silico Medicine (P.C.E.), University of Sheffield, Sheffield, United Kingdom; and Division of Cardiovascular Medicine, University of Cambridge, Cambridge, United Kingdom (M.R.B.).

The online-only Data Supplement is available with this article at <http://atvb.ahajournals.org/lookup/suppl/doi:10.1161/ATVBAHA.114.303415/-DC1>.

Correspondence to Paul C. Evans, PhD, Department of Cardiovascular Science, Faculty of Medicine, Dentistry and Health, University of Sheffield, Medical School, Beech Hill Rd, Sheffield S10 2RX, United Kingdom. E-mail paul.evans@sheffield.ac.uk

© 2014 American Heart Association, Inc.

*Arterioscler Thromb Vasc Biol* is available at <http://atvb.ahajournals.org>

DOI: 10.1161/ATVBAHA.114.303415

**Nonstandard Abbreviations and Acronyms**

<b>C<sub>12</sub>FDG</b>	dodecanoyleaminofluorescein di-β-galactopyranoside
<b>EC</b>	endothelial cell
<b>ICAM-1</b>	intercellular adhesion molecule-1
<b>SA-β-gal</b>	senescence-associated β-galactosidase

leading to inhibition of E2F transcription factors and expression of genes required for G1/S transition. Of note, the relative contribution of the p53-p21 and p16 tumor suppressor pathways to replicative and stress-induced senescence is a topic of much debate.

Cellular senescence is now attracting considerable interest in the cardiovascular field. Several studies have shown that telomere lengths in white blood cells are shorter in patients with atherosclerosis<sup>9–15</sup> compared with healthy controls, suggesting that replicative senescence may be involved in this disease. Moreover, telomere lengths decline with age in human arteries<sup>16–18</sup> and are shorter in coronary and carotid artery plaques compared with healthy vessels.<sup>3,19,20</sup> Increased activity of senescence-associated β-galactosidase (SA-β-gal) is commonly used to identify senescent cells.<sup>21</sup> Senescent cells are also associated with alterations in cellular morphology including enlargement, flattening, and multinucleation. Several studies have identified SA-β-gal-positive<sup>22–24</sup> or giant, multinucleated endothelial cells (ECs) overlying atherosclerotic plaques.<sup>25–28</sup> EC senescence can be induced in arteries by repeated injury (presumably through replicative exhaustion)<sup>29</sup> and in response to various proatherogenic factors including tumor necrosis factor-α, reactive oxygen species, oxidized low-density lipoprotein, and angiotensin II.<sup>3,4,30–32</sup> By contrast, growth factors<sup>33,34</sup> and NO<sup>22,35</sup> protect ECs from entering the senescent state. Despite these insights, the molecular mechanisms that promote EC senescence in arteries and the role, if any, of senescent ECs in atherosclerosis are largely unknown.

Although atherosclerosis is associated with systemic risk factors such as age, high cholesterol, and obesity, plaque formation occurs predominately at branches and bends, whereas regions of uniform geometry are protected.<sup>36,37</sup> The velocity and direction of blood flow, which varies according to vascular geometry and pulsatility, exhibits greater variation at atheroprone sites compared with protected regions. For example, biaxial or secondary flows are more prominent at atheroprone compared with protected sites.<sup>36,37</sup> For the sake of brevity, we refer to flow patterns at atheroprone sites as disturbed and flow at protected sites as undisturbed. Here, we demonstrated that disturbed blood flow promotes EC senescence by activating p53-p21 signaling. Flow-induced senescent ECs had a reduced capacity for migration and displayed abnormal expression of inflammatory molecules, suggesting that they may be involved in vascular injury. Finally, we identified a potential intervention to suppress flow-induced senescence by demonstrating that this process can be inhibited by pharmacological activation of sirtuin 1.

**Materials and Methods**

Materials and Methods are available in the online-only Supplement.<sup>38–43</sup>

**Results**

Although senescent ECs have been identified overlying atherosclerotic plaques, their potential role in plaque initiation and progression is uncertain. To address this, we quantified SA-β-gal-positive cells in en face preparations of aortae isolated from LDLR<sup>-/-</sup> mice. SA-β-gal staining at the aortic root, along the inner curvature, and at the major branches of the aortic arch was minimal in mice fed a normal chow diet but was enhanced in response to exposure to a high-fat diet for 2 to 12 weeks (Figure 1A). To confirm that SA-β-gal-positive cells were of endothelial origin, a fluorescent SA-β-gal substrate, dodecanoyleaminofluorescein di-β-galactopyranoside (C<sub>12</sub>FDG), was used in conjunction with rhodamine-conjugated Griffonia lectin to identify ECs. En face staining revealed that the intensity of C<sub>12</sub>FDG was greater at the inner curvature (an atheroprone area exposed to disturbed flow) compared with the outer curvature (undisturbed flow region) and that the C<sub>12</sub>FDG signal was enhanced by exposure to a high-fat diet (Figure 1B). Similarly, en face staining studies in LDLR<sup>-/-</sup> mice demonstrated that high-fat feeding enhanced endothelial expression of p53 at the inner curvature but not at the outer curvature (Figure 2). By contrast, p16 was not detected in murine aortae (data not shown). Studies using porcine aortae ( $\approx$ 6 months old) revealed SA-β-gal-positive staining at sites of disturbed flow including the origin of the left subclavian artery and brachiocephalic trunk and along the inner curvature of the aortic arch (Figure 1A in the online-only Data Supplement). SA-β-gal-positive staining was confirmed to be of endothelial origin by taking Häutchen preparations of the luminal layer (Figure 1B in the online-only Data Supplement). These data suggest that senescent ECs accumulate at sites of disturbed flow.

Our *in vivo* observations led us to hypothesize that disturbed flow may promote EC senescence. To test this, we used an orbital shaking platform which generates reproducible spatially separated biaxial (disturbed) and uniaxial pulsatile (undisturbed) flow patterns.<sup>40–42</sup> CFD analysis demonstrated that orbital shaking generated wall shear stress at the center of the well that had a relatively constant low magnitude but varied rapidly in direction (Figure 3A). Conversely, the periphery was associated with temporal fluctuations in the magnitude of wall shear stress, a relatively high maximum wall shear stress and relatively uniform direction (Figure 3A). We validated the orbital flow system by measuring the expression of transcripts that are known to be induced by disturbed (E-selectin) or undisturbed (endothelial NO synthase) flow. Cells at the center of orbiting wells expressed relatively high levels of E-selectin and low levels of endothelial NO synthase, whereas ECs at the periphery exhibited the opposite pattern (Figure 3B). Moreover, cells in the central region were not aligned, whereas cells in the periphery were elongated and aligned in the direction of the flow (Figure 3C) as described previously.<sup>41,42</sup> We conclude that the orbital flow system generates spatially distinct flow fields and that cells in the center display morphological and transcriptional features that are characteristic of the response to disturbed flow. We used the orbital shaker platform to determine whether the application of disturbed or undisturbed flow for 72 hours can influence

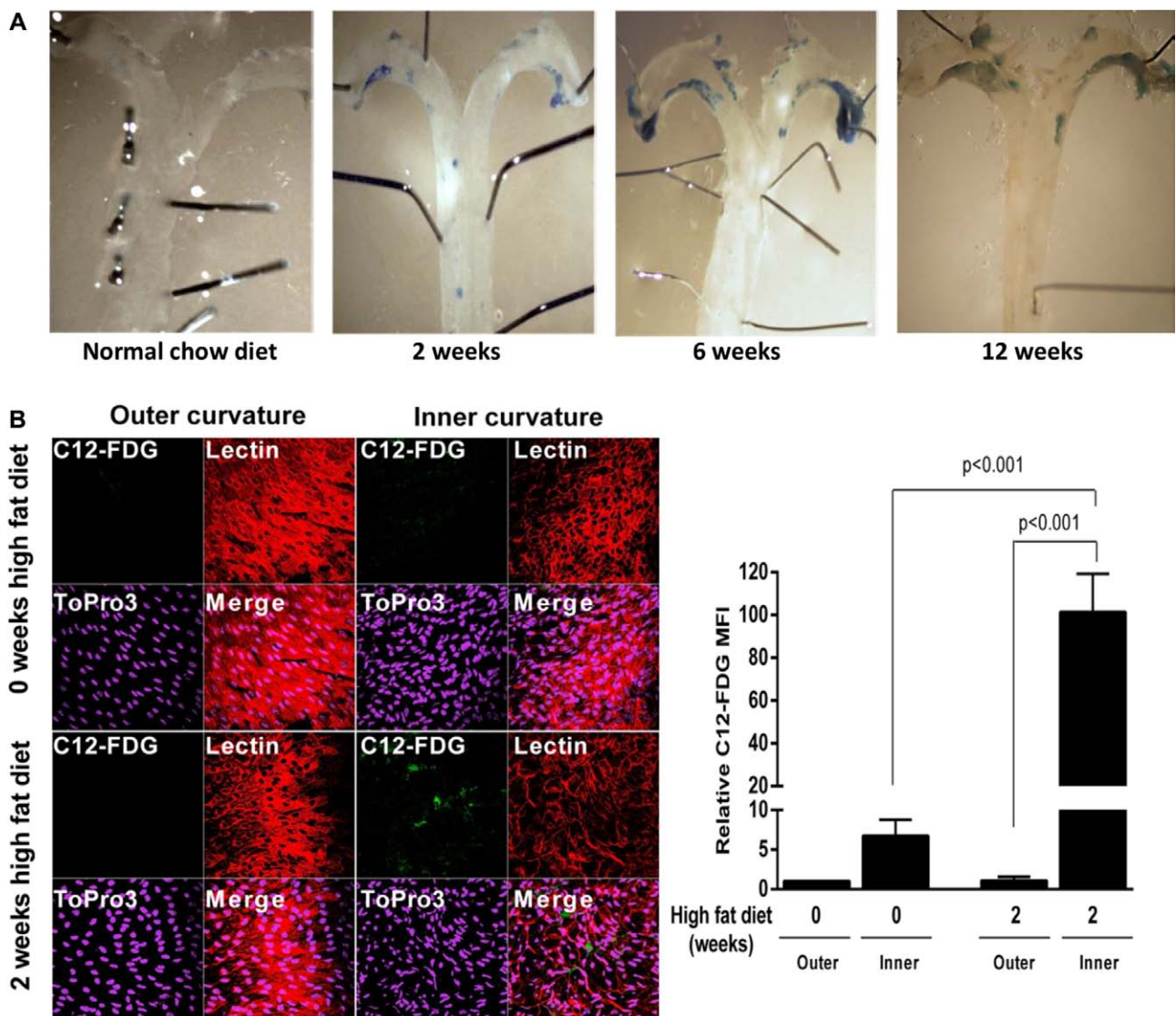


**Figure 1.** Senescence-associated  $\beta$ -galactosidase (SA- $\beta$ -gal)-positive endothelial cells (ECs) were identified at atherosusceptible sites. **A**,  $LDLR^{-/-}$  mice (aged 10 weeks) were fed a normal chow diet or high-fat diet for 2 to 12 weeks. **B**, Aortae were assessed by colorimetric SA- $\beta$ -gal staining or by en face staining of the outer (undisturbed flow) and inner (disturbed flow) curvature using dodecanoylaminofluororescein di- $\beta$ -galactopyranoside ( $C_{12}$ -FDG; green), Griffonia lectin (red), and ToPro-3 (purple).  $C_{12}$ -FDG fluorescence at undisturbed and disturbed sites was quantified, and data were pooled from 5 independent experiments. MFI indicates mean fluorescence index.

senescence in cultured human umbilical vein ECs or porcine aortic ECs. The percentage of large, SA- $\beta$ -gal-positive (senescent) cells was significantly higher at the disturbed flow region compared with the undisturbed flow region or compared with static cultures in both venous and arterial ECs (Figure 3C and Figure II A in the online-only Data Supplement). Similarly, studies using syringe-pump flow bioreactor systems revealed that oscillatory flow induced cells that were SA- $\beta$ -gal positive, large, and multinucleated, whereas undisturbed flow did not (Figure II B and II C in the online-only Data Supplement). Thus, we conclude that EC senescence can be promoted by disturbed flow.

Flow can influence EC proliferation.<sup>43–45</sup> Thus, we hypothesized that disturbed flow may induce EC senescence by promoting endothelial proliferation and consequent replicative exhaustion. To assess this, ECs were exposed to disturbed or undisturbed flow and proliferating cells were quantified by

immunofluorescent staining using antibodies that recognize a marker of proliferation (Ki67; Figure III A in the online-only Data Supplement) or by measuring incorporation of EdU, a fluorescent thymidine analogue (data not shown). ECs exposed to disturbed or undisturbed flow for 6 to 72 hours exhibited similar rates of proliferation (Figure III A in the online-only Data Supplement) and cell counts (Figure III B in the online-only Data Supplement), indicating that senescence did not result from increased proliferation at the disturbed flow site.

We examined the potential role of p53 in senescence because this transcription factor can be induced by disturbed flow<sup>46</sup> and it was expressed at a disturbed flow site in the murine aorta (Figure 2). Single-cell analysis of proteins levels by immunofluorescent staining revealed that p53 and p21 expression was strikingly elevated in senescent ECs compared with nonsenescence cells (exposed to either disturbed or

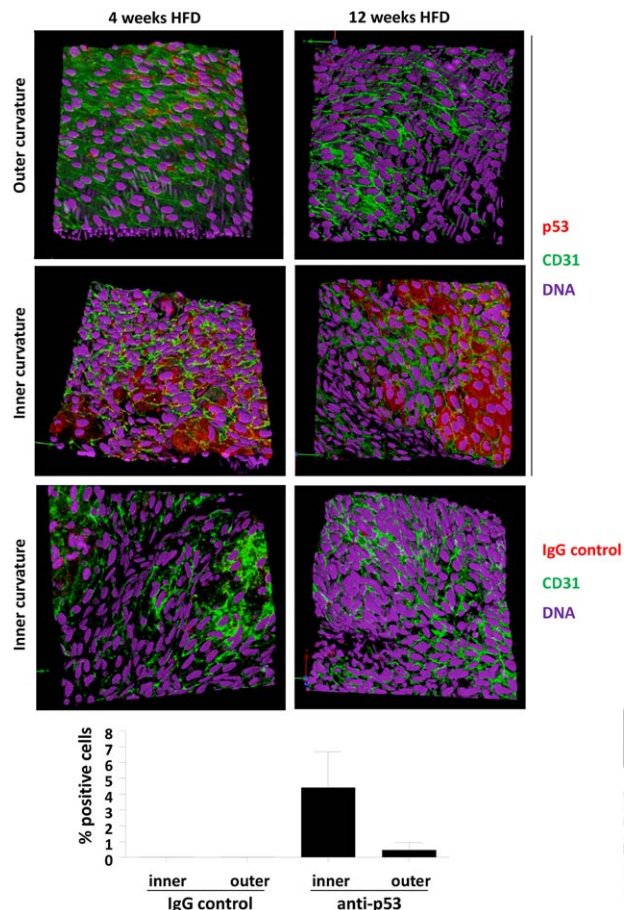


**Figure 2.** Large, p53-positive endothelial cells (ECs) were identified at atherosusceptible sites. *LDLR*<sup>-/-</sup> mice (aged 10 weeks) were fed a normal chow diet or high-fat diet (HFD) for 4 or 12 weeks. The expression of p53 was measured in ECs by en face staining of susceptible or protected regions of the aorta (red; n=6 per group) followed by laser scanning confocal microscopy. Endothelial marker is CD31 (green), and nuclei were stained using ToPro-3 (purple). z-stacks were converted into 3-dimensional images using ImageJ software. Representative images and quantitation of p53-positive cells (mean±SD) are shown.

undisturbed flow; Figure 4A), and costaining revealed that p53 and p21 were coexpressed in senescent ECs (Figure 4B). Thus, the highest expression of p53 and p21 was restricted to senescent ECs exposed to disturbed flow. The mechanism is unlikely to involve changes at the transcript level because p53 mRNA levels were similar in ECs exposed to flow (disturbed or undisturbed) or static conditions, whereas p21 expression was elevated by undisturbed flow (Figure IV in the online-only Data Supplement). The function of p53 and p21 was determined by gene silencing, which was confirmed by quantitative real-time polymerase chain reaction (Figure VA and VB in the online-only Data Supplement). In cultures exposed to disturbed flow, silencing of p53 (Figure 4C) or p21 (Figure 4D) significantly reduced the incidence of senescent cells. Interestingly, gene silencing revealed that p53 and p21 also positively regulated senescence in ECs exposed to static conditions or undisturbed flow, albeit at lower levels than under disturbed flow conditions (Figure 4C and 4D). Silencing of p53 reduced the expression of p21 in ECs (Figure 4E), indicating that p53 acts upstream of p21. Collectively, these data

suggest that disturbed flow promotes EC senescence by activating a p53-p21 signaling pathway and that this pathway also influences the fate of cells exposed to undisturbed flow.

To assess the behavior and function of senescent ECs, we assessed their migratory capacity using the scratch wound healing assay coupled to live cell imaging. Human umbilical vein ECs were exposed to flow for 72 hours and then imaged under static conditions. Senescent ECs induced by disturbed flow migrated more slowly than surrounding non-senescent cells (Figure 5A). Therefore, the accumulated and Euclidean distance migrated by senescent cells during the imaging period was significantly less when compared with the migration distance of surrounding non-senescent cells (Figure 5B and 5C). Senescent ECs also impeded the migration of neighboring cells, whereas non-senescent cells did not (Figure 5A and 5C). These data indicate that senescent ECs have a reduced migratory capacity and also impede the migration of surrounding healthy cells. We conclude, therefore, that senescent ECs may impair wound healing and vascular repair in areas of disturbed flow.

The inflammatory phenotype of senescent ECs induced by disturbed flow was also assessed. Immunofluorescent staining was used to measure the expression of inflammatory adhesion molecules in senescent ECs in both basal conditions and after exposure to the inflammatory cytokine tumor necrosis factor- $\alpha$ . After staining for intercellular adhesion molecule-1 (ICAM-1), the mean fluorescence index (proportionate to the concentration of ICAM-1 over a given area of cell membrane) under either basal conditions or after tumor necrosis factor- $\alpha$  treatment was reduced in senescent ECs (p21 positive, large) compared with non-senescent cells (Figure 5D and 5E). Interestingly, the total levels of ICAM-1 expressed in senescent ECs (calculated as mean fluorescence index $\times$ cell area) were similar to total ICAM-1 levels in healthy ECs (Figure VIB in the online-only Data Supplement). Similarly, the expression level of vascular cell adhesion molecule-1 per cell was similar in senescent and healthy cells, but the mean fluorescence index was reduced in the senescent population (Figure VIA in the online-only Data Supplement). Thus, senescent and healthy ECs expressed similar levels of ICAM-1 and vascular cell adhesion molecule-1, but the concentration of these adhesion molecules was reduced in the former, possibly because they are distributed over a greater cell surface area. Our observation suggests disturbed flow-induced senescent ECs may be dysfunctional in terms of leukocyte recruitment by expressing lower concentrations of ICAM-1 and vascular cell adhesion molecule-1.

We examined whether the induction of senescence in ECs exposed to flow was regulated by sirtuin 1, a deacetylase that can function as a negative regulator of p53 signaling in some cell types. Silencing of sirtuin 1 (Figure 6A and Figure VC in the online-only Data Supplement) or pharmacological inhibition of sirtuins (using the inhibitor sirtinol; Figure 6B) promoted senescence in cells exposed to undisturbed flow but did not influence cells cultured under disturbed flow. We therefore concluded that sirtuin 1 protects ECs exposed to undisturbed flow from the induction of senescence. By contrast, we reasoned that ECs exposed to disturbed flow may be susceptible

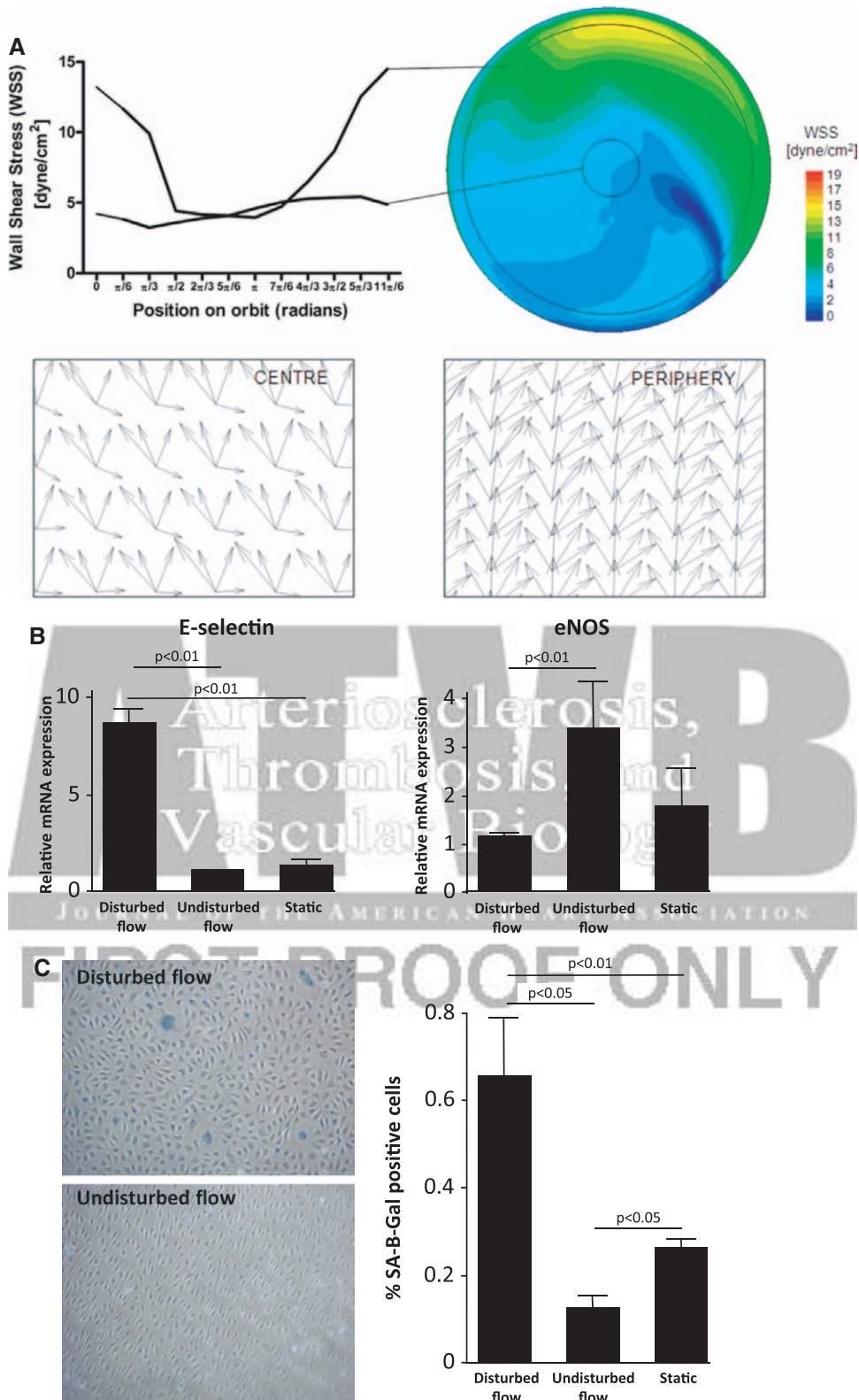


**Figure 3.** Disturbed flow promotes endothelial cell (EC) senescence. **A**, Wall shear stress (WSS) magnitude ( $\text{dyne}/\text{cm}^2$ ) acting on central and peripheral regions of an orbiting 6-well plate (210 rpm; 3-mL cell culture medium/well) throughout 1 orbit (**upper left**) and map of shear stress magnitude at a single time point (**upper right**) are shown. Velocity vectors at 4 subsequent time points in central (**lower left**) and peripheral (**lower right**) regions are presented. **B** and **C**, Human umbilical vein ECs were exposed to orbital flow for 72 hours or to static conditions as a control. **B**, E-selectin and endothelial NO synthase (eNOS) transcript levels were quantified by quantitative real-time polymerase chain reaction. Mean values pooled from 3 independent experiments are shown with SDs. **C**, Senescent cells were detected using the senescence-associated  $\beta$ -galactosidase (SA- $\beta$ -gal) assay at regions of disturbed (center) or undisturbed (periphery) flow. Representative staining is shown (**left**). The percentage of SA- $\beta$ -gal-positive cells was calculated in multiple fields of view per region of 4 independent experiments, and mean values are shown with SDs (**right**).

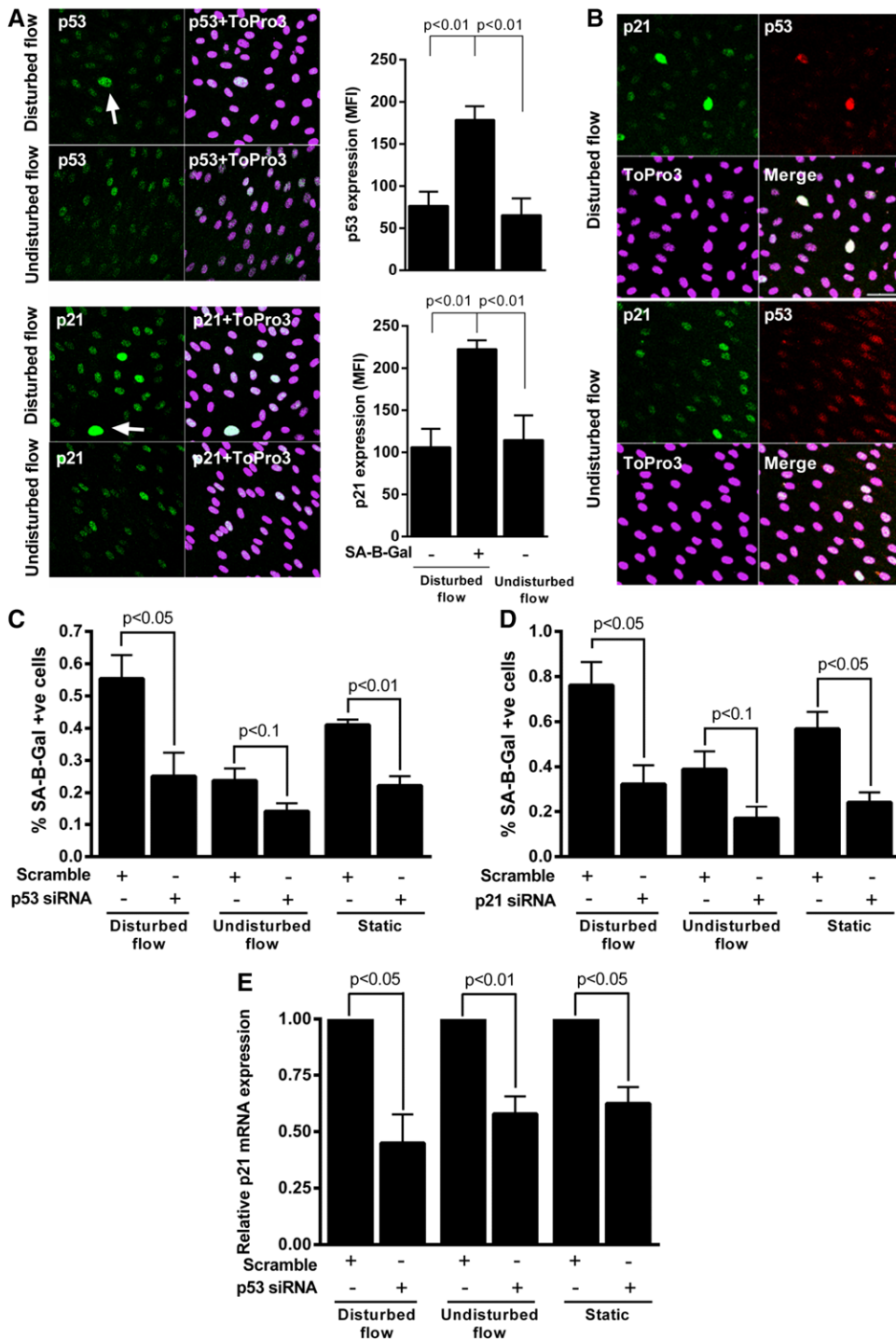


**Figure 4.** Flow-induced senescence requires activation of p53 and p21 human umbilical vein endothelial cells (HUVECs) were exposed to orbital flow for 72 hours or to static conditions as a control. **A**, Immunofluorescent staining was performed using anti-p53 (green; **upper**) or anti-p21 (green; **lower**) antibodies and nuclei were counterstained using ToPro-3 (purple). Staining for senescence-associated  $\beta$ -galactosidase (SA- $\beta$ -gal) was conducted in parallel, and positive cells are marked by arrows. Fluorescence of cells exposed to disturbed (center) or undisturbed (periphery) flow was assessed by laser scanning confocal microscopy, and representative images are shown. The expression of p53 and p21 in SA- $\beta$ -gal-positive or SA- $\beta$ -gal-negative cells at regions of disturbed flow (or in cells exposed to undisturbed flow) was quantified, and data from 4 independent experiments were pooled. Mean fluorescence values are shown with SEs. **B**, Costaining using anti-p53 (red) and anti-p21 (green) antibodies was performed. Nuclei were counterstained with ToPro-3 (purple). Fluorescence of cells exposed to disturbed (center) or undisturbed (periphery) flow was assessed by laser scanning confocal microscopy, and representative images are shown. Scale bar (bottom right) shows 50  $\mu$ m. Rates of disturbed flow-induced senescence were assessed in HUVECs transfected with small interfering RNA (siRNA) targeting p53 (**C**) or p21 (**D**) relative to scramble-treated controls using the SA- $\beta$ -gal assay. Mean values were pooled from 3 independent experiments and are shown with SDs. **E**, p21 expression was assessed by quantitative real-time polymerase chain reaction in sheared HUVECs transfected with p53 siRNA or nontargeting (scrambled) siRNA. Mean values pooled from 3 independent experiments are shown with SDs. MFI indicates mean fluorescence index.

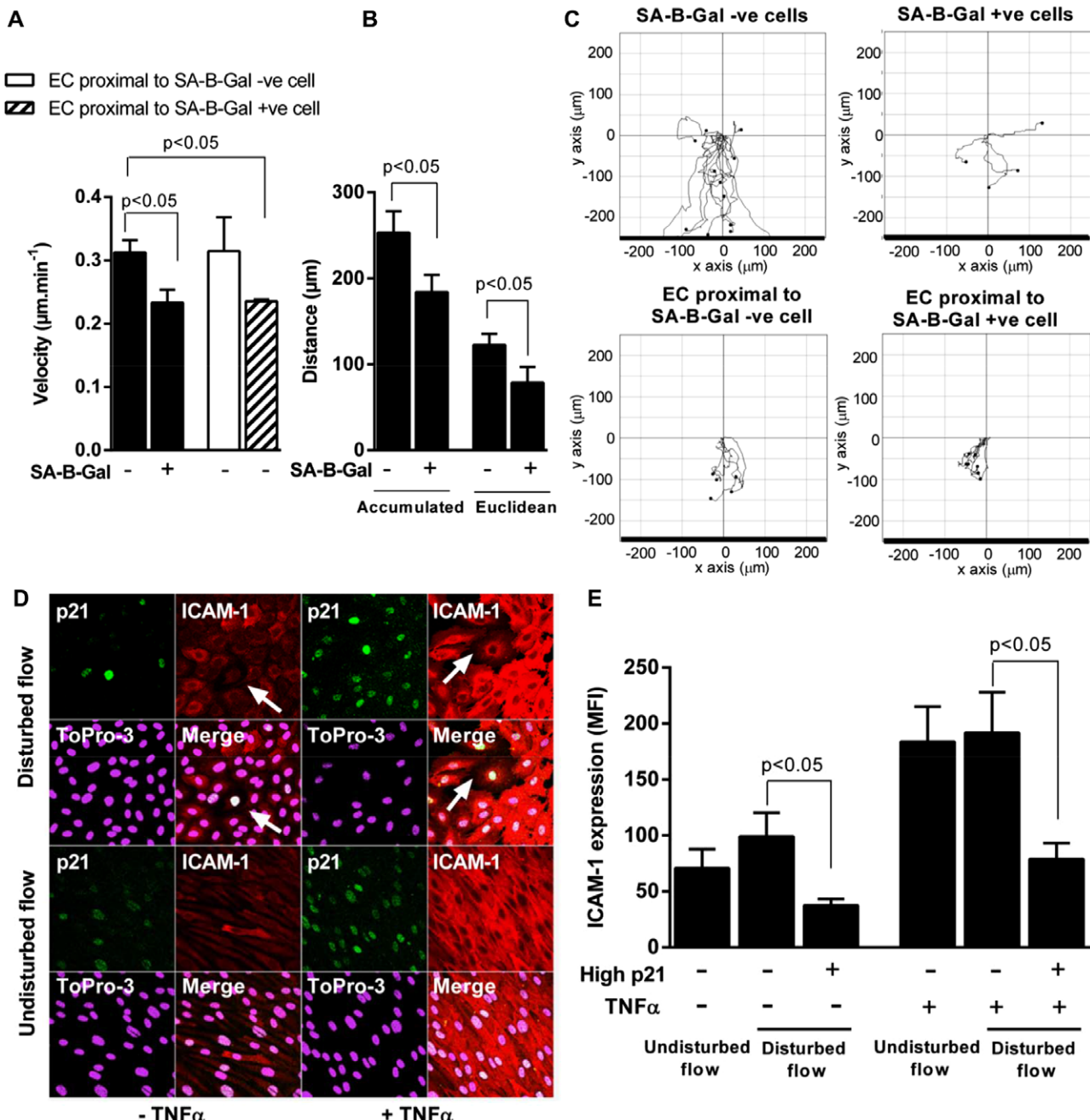


**Figure 5.** Disturbed flow-induced senescent endothelial cells (ECs) migrate less and exhibit reduced inflammatory activation. **A** to **C**, Human umbilical vein ECs (HUVECs) were exposed to disturbed flow for 72 hours. A scratch wound was then performed and superimposed onto the live cell imaging data. This allowed migration trajectories to be plotted for SA- $\beta$ -gal-positive (senescent) and SA- $\beta$ -gal-negative (healthy) cells using ImageJ software (**C**, upper). Trajectories were also calculated for healthy cells located proximal to either SA- $\beta$ -gal-positive or SA- $\beta$ -gal-negative cells (**C**, lower). Migration trajectories were used to calculate the migration velocities (**A**) and accumulated and Euclidean distances (**B**). The migration trajectories of  $\approx$ 50 individual cells per experiment were assessed. Data were pooled from 4 independent experiments. **D** and **E**, HUVECs exposed to disturbed flow for 72 hours were exposed to tumor necrosis factor- $\alpha$  (TNF- $\alpha$ ; 10 ng/mL for 18 hours) or remained untreated before costaining of intercellular adhesion molecule-1 (ICAM-1; red) and p21 (green). Nuclei were stained with ToPro-3 (purple). Staining for SA- $\beta$ -gal was conducted in parallel, and positive cells are marked by arrows. **D**, Representative images are shown. **E**, ICAM-1 mean fluorescence was calculated for senescent (SA- $\beta$ -gal/p21 positive) and nonsenescent (SA- $\beta$ -gal/p21 negative) cells, and mean values are shown with SEs. Data were pooled from 4 independent experiments. MFI indicates mean fluorescence index.

to senescence because they express relatively low levels of sirtuin 1 (compared with cells exposed to undisturbed flow). To address this hypothesis, we used resveratrol, a polyphenol that is known to induce sirtuin 1 expression,<sup>47</sup> and SRT1720,

which is a specific activator of sirtuin 1. Pretreatment of ECs using resveratrol (100  $\mu\text{mol/L}$ ) reduced the subsequent induction of senescent ECs by disturbed flow (Figure 6C). Suppression of sirtuin 1 by treatment with sirtinol (Figure 6D)

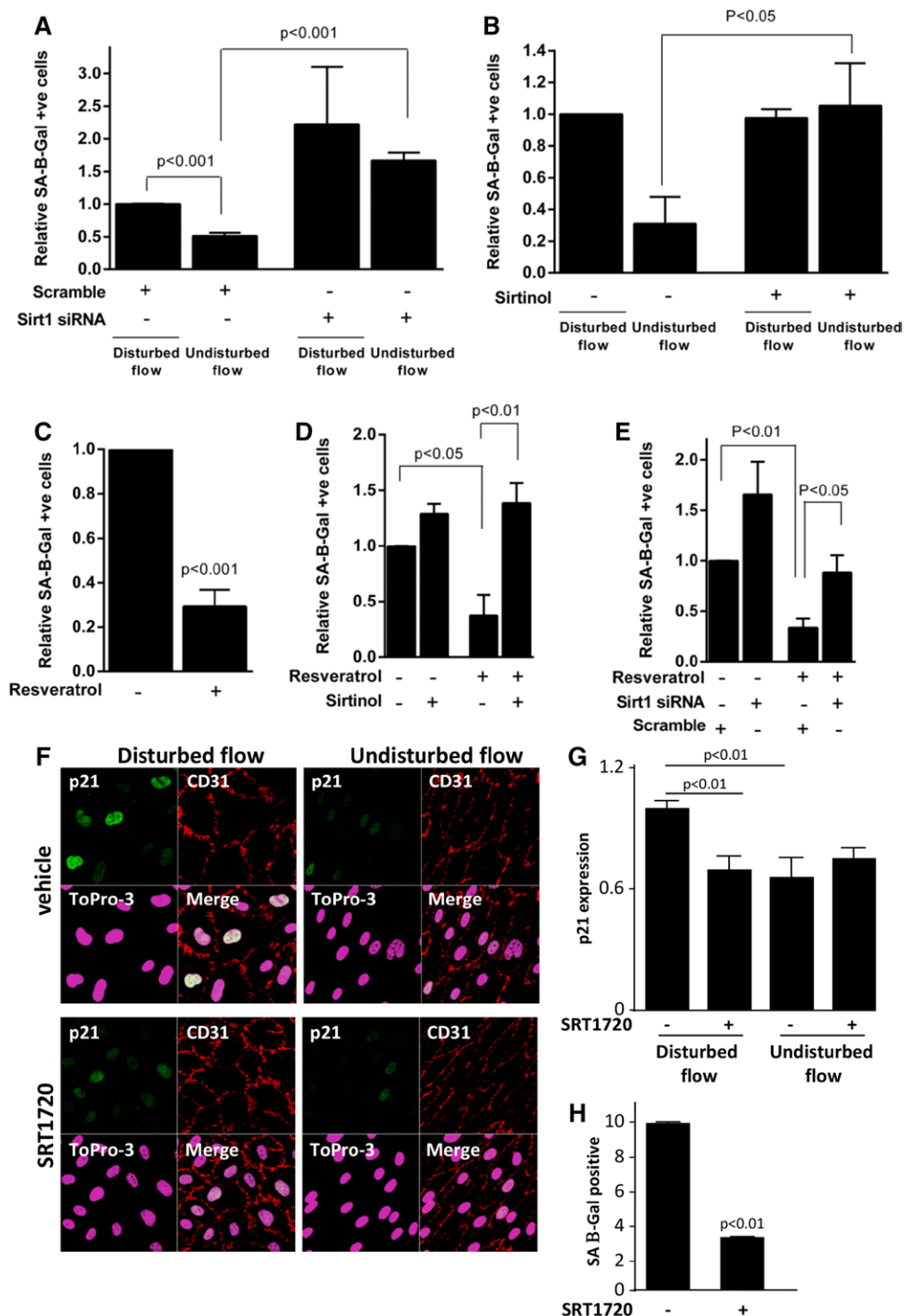


**Figure 6.** Pharmacological activation of sirtuin 1 (Sirt1) protects endothelial cells (ECs) from senescence in response to disturbed flow. **A** and **B**, Human umbilical vein ECs (HUVECs) were transfected with Sirt1 small interfering RNA (siRNA) or scrambled sequences (100 nmol/L final concentration), or were treated with sirtinol (50 μmol/L) or with vehicle alone. Cells were then exposed to disturbed or undisturbed flow for 72 hours. Senescence rates were measured using the senescence-associated β-galactosidase (SA-β-gal) assay. Data were pooled from ≥3 independent experiments, and mean values are shown with SEs. **C**, HUVECs were treated with resveratrol (100 μmol/L) or with vehicle alone immediately before the application of disturbed flow for 72 hours. Senescence rates were measured using the SA-β-gal assay. Data were pooled from 6 independent experiments, and mean values are shown with SEs. **D** and **E**, HUVECs were pretreated with sirtinol (50 μmol/L) or with vehicle alone (**D**) or were transfected with Sirt1 siRNA or with a scrambled control (**E**). Cells were subsequently treated with resveratrol (100 μmol/L) or with vehicle alone before the application of disturbed flow for 72 hours. Senescence rates were measured using the SA-β-gal assay. Data were pooled from 3 independent experiments, and mean values are shown with SEs. **F** to **H**, HUVECs were treated with SRT1720 (20 μmol/L) or with vehicle alone immediately before the application of disturbed or undisturbed flow for 72 hours. **G** and **H**, Immunofluorescent staining was performed using anti-p21 antibodies (green), and ECs were identified using anti-CD31 antibodies (red). Nuclei were counterstained using ToPro-3 (purple). Fluorescence of cells exposed to disturbed or undisturbed flow was assessed by laser scanning confocal microscopy. **F**, Representative images are shown. **G**, The expression of p21 was quantified in multiple ECs, and data from 3 independent experiments were pooled. Mean fluorescence values are shown with SDs. **H**, Senescence rates were measured using the SA-β-gal assay. Data were pooled from 3 independent experiments, and mean values are shown with SDs.

or by gene silencing (Figure 6E) restored the induction of EC senescence by disturbed flow in resveratrol-treated cells, indicating that resveratrol protects ECs via sirtuin 1. Similarly, it was concluded that SRT1720 can protect ECs from senescence because treatment using this compound significantly reduced the induction of p21 (Figure 6F and 6G) and activation of SA- $\beta$ -gal (Figure 6H) in response to disturbed flow. Therefore, pharmacological induction of sirtuin 1 can suppress the induction of senescence by disturbed flow.

## Discussion

Senescent ECs have previously been identified in advanced plaques,<sup>22–24</sup> but it is uncertain whether they influence early atherogenesis. We demonstrate here that ECs overlying early atherosclerotic lesions display several features that are characteristic of cellular senescence; specifically, they were enlarged, displayed high SA- $\beta$ -gal activity, and expressed high levels of p53. The corollary to these observations is that EC senescence may be involved in atherosclerosis initiation and progression and may contribute to the focal nature of the disease. EC senescence can be induced in arteries by oxidized low-density lipoprotein, tumor necrosis factor- $\alpha$ , and other proatherogenic molecules.<sup>3,4,30–32</sup> The presence of senescent ECs at atheroprone sites in vivo may be related to local hemodynamics because we observed that senescent ECs accumulate under disturbed flow (but not undisturbed flow) conditions in vitro. We hypothesized that disturbed flow induces senescence as a consequence of enhanced proliferation because ECs at atheroprone sites display relatively high rates of turnover compared with those at protected sites.<sup>43,44</sup> Although replicative senescence may occur at atheroprone sites in vivo, we observed that disturbed flow can induce senescence in the absence of increased cell turnover. These data imply that the senescent phenotype may be induced in ECs as a direct consequence of flow perturbation. The focal nature of EC senescence is related to wall shear stress, a force exerted on ECs by flowing blood that varies in time, magnitude, and direction according to vascular pulsatility and anatomy.<sup>36,48,49</sup> Shear stress influences many aspects of EC physiology,<sup>36,37,48–50</sup> and future studies should now be performed to examine whether mechanical stimulation can trigger the induction of senescence. This concept is novel because mechanical forces have not been previously linked to vascular aging processes. Interestingly, disturbed flow was sufficient to induce endothelial senescence in vitro, whereas senescent cells were induced at disturbed flow sites in vivo by high-fat feeding. Thus, although disturbed flow was involved in the induction of senescence in vivo, it was not sufficient to induce growth arrest in the absence of other cues. It is plausible that the generation of senescent cells in a disturbed flow environment requires a second stress signal. This signal may be present in vitro because cell isolation and culture is associated with physiological stresses (eg, hyperoxia). By contrast, ECs exposed to disturbed flow may receive a second stress signal in response to hypercholesterolemia. Disturbed flow has been shown to influence several functions including morphology, inflammatory activation, and apoptosis.<sup>36,37</sup> Our observation that proliferating and senescent ECs coexist at sites of disturbed flow reinforces the concept

that atheroprone sites are associated with considerable heterogeneity in cell phenotype.<sup>36</sup>

Using a combination of immunostaining and gene silencing, we demonstrated that p53 and p21 activation were required for disturbed flow-induced senescence. These findings provide further evidence of the diversity and complexity of senescence induction. They align with previous studies demonstrating that the contribution of p53, p21, and p16 varies with the type of stimulus.<sup>5–8</sup> p53 coordinates the cellular response to stress and is a key regulator of cell fate. Interestingly, previous studies revealed that p53 and p21 are activated by both disturbed and undisturbed flow, although the effects on cell fate were dissimilar. Undisturbed flow induces reversible growth arrest (quiescence) and protection from apoptosis via p53-mediated induction of p21 and GADD45.<sup>45,51,52</sup> Other studies have shown that disturbed flow promotes apoptosis via a mechanism that involves modification of p53 with SUMO and retention in the cytoplasm.<sup>46</sup> Together with our current study, which indicated a role for p53 in disturbed flow-induced senescence, these observations emphasize the pleiotropic nature of p53 which is influenced by blood flow patterns. Further studies should be performed to identify the molecular mechanisms that control p53 decision making in sheared ECs.

Senescent cells remain metabolically active and often acquire an altered transcriptional profile. As a consequence, they have the potential to modify the function of tissues in which they accumulate. Here, we demonstrate for the first time that senescent ECs migrate more slowly than surrounding nonsenescent ECs exposed to the same mechanical environment. This suggests that regions of the arterial tree where senescent cells accumulate may have an impaired capacity to repair. This has important implications in vivo in the context of plaque progression because dysfunctional repair mechanisms may promote local inflammatory activation and thrombosis. Senescent ECs can be considered proatherogenic in this regard. Paradoxically, although senescence has been associated with inflammation in other contexts, the induction of EC senescence by disturbed flow was associated with a reduced expression of ICAM-1 and vascular cell adhesion molecule-1 at the cell surface, suggesting potential antiatherogenic properties. These findings support recent observations that H<sub>2</sub>O<sub>2</sub>-induced senescent ECs, mediated via activation of the SENEX gene, express lower levels of proinflammatory proteins.<sup>3</sup> These observations emphasize the need for further research into the potential role of senescent ECs in atherosclerosis which is likely to be complex.

The NAD<sup>+</sup>-dependent deacetylase sirtuin 1 negatively regulates p53<sup>53–57</sup> by removing acetyl groups, thus enhancing p53 degradation via the ubiquitin ligase Mdm2. We observed using a small interfering RNA-based approach or using a pharmacological inhibitor (sirtinol) that sirtuin 1 protects against the induction of senescence in ECs which is consistent with a previous report.<sup>54</sup> Notably, pretreatment of ECs using resveratrol, found in grapes and red wine, inhibited senescence in response to disturbed flow via a sirtuin 1-dependent mechanism. Pretreatment with resveratrol also caused ECs in disturbed flow regions, which typically exhibit polygonal, cobblestone morphology, to become elongated

(data not shown). We reason that this may be because of the actions of resveratrol on Krüppel-like factor 2<sup>58</sup> which has previously been shown to cause elongation of ECs under static conditions.<sup>59</sup> Although resveratrol can exert cardioprotective effects,<sup>60–62</sup> the physiological significance of these effects has been doubted because of its low bioavailability.<sup>63</sup> Nevertheless, our observations support the principle that pharmacological activation of sirtuin 1 may promote cardiovascular health by suppressing EC senescence at atherosprone sites. This concept is further substantiated by our observation that an alternative sirtuin 1 activator (SRT1720) can also reduce the induction of senescence by disturbed flow. We speculate that the mechanism may involve sirtuin 1–dependent deacetylation and deactivation of p53 to prevent cell cycle arrest; however, other possibilities exist because sirtuin 1 also negatively regulates cell cycle arrest by suppressing liver kinase B1/AMPK<sup>55</sup> and nuclear factor κB<sup>56</sup> and by inducing NO.<sup>54,57</sup> Our observations reveal a novel mechanism for the protective effects of sirtuin 1 in vascular ECs. They are consistent with previous reports that sirtuin 1 can protect against lesion formation in atherosclerosis-prone mice<sup>64,65</sup>; however, further studies using conditional sirtuin 1 knockouts are now required to define the cell types that are responsible for the protective effects of sirtuin 1 activation *in vivo*.

## Sources of Funding

This work was funded by the British Heart Foundation.

## Disclosures

None.

## References

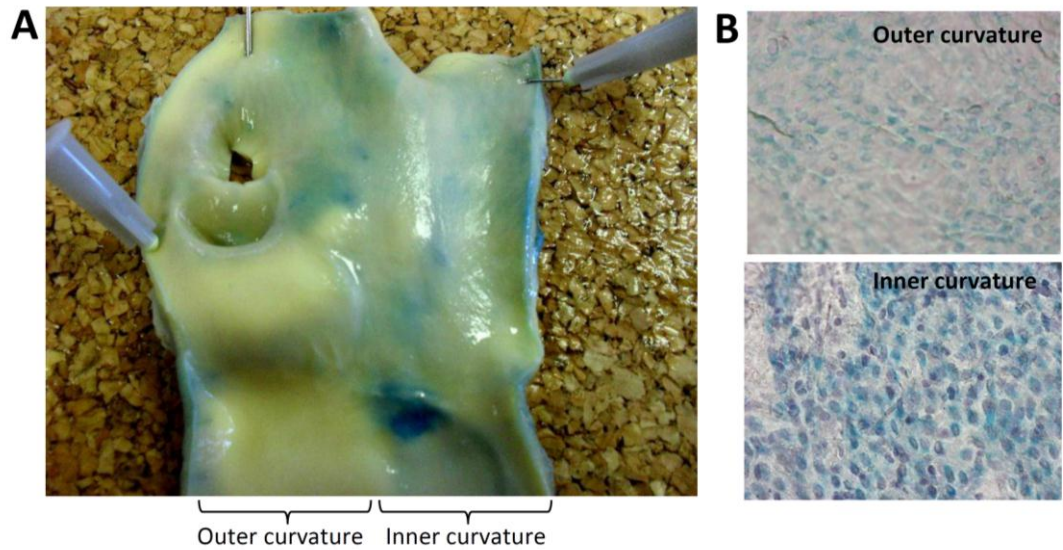
- Hayflick L, Moorhead PS. The serial cultivation of human diploid cell strains. *Exp Cell Res.* 1961;25:585–621.
- Harley CB, Futcher AB, Greider CW. Telomeres shorten during ageing of human fibroblasts. *Nature.* 1990;345:458–460.
- Coleman PR, Hahn CN, Grimshaw M, Lu Y, Li X, Brautigan PJ, Beck K, Stocker R, Vadas MA, Gamble JR. Stress-induced premature senescence mediated by a novel gene, SENEX, results in an anti-inflammatory phenotype in endothelial cells. *Blood.* 2010;116:4016–4024.
- Haendeler J, Hoffmann J, Diehl JF, Vasa M, Spyridopoulos I, Zeiher AM, Dimmeler S. Antioxidants inhibit nuclear export of telomerase reverse transcriptase and delay replicative senescence of endothelial cells. *Circ Res.* 2004;94:768–775.
- Serrano M, Lin AW, McCurrach ME, Beach D, Lowe SW. Oncogenic ras provokes premature cell senescence associated with accumulation of p53 and p16INK4a. *Cell.* 1997;88:593–602.
- Beauséjour CM, Krtolica A, Galimi F, Narita M, Lowe SW, Yaswen P, Campisi J. Reversal of human cellular senescence: roles of the p53 and p16 pathways. *EMBO J.* 2003;22:4212–4222.
- d'Adda di Fagagna F, Reaper PM, Clay-Farrace L, Fiegler H, Carr P, von Zglinicki T, Saretzki G, Carter NP, Jackson SP. A DNA damage checkpoint response in telomere-initiated senescence. *Nature.* 2003;426:194–198.
- Herbig U, Jobling WA, Chen BP, Chen DJ, Sedivy JM. Telomere shortening triggers senescence of human cells through a pathway involving ATM, p53, and p21(CIP1), but not p16(INK4a). *Mol Cell.* 2004;14:501–513.
- Benetos A, Gardner JP, Zureik M, Labat C, Xiaobin L, Adamopoulos C, Temmar M, Bean KE, Thomas F, Aviv A. Short telomeres are associated with increased carotid atherosclerosis in hypertensive subjects. *Hypertension.* 2004;43:182–185.
- Brouilette S, Singh RK, Thompson JR, Goodall AH, Samani NJ. White cell telomere length and risk of premature myocardial infarction. *Arterioscler Thromb Vasc Biol.* 2003;23:842–846.
- Kurz DJ, Kloeckner-Gruissem B, Akhmedov A, Eberli FR, Bühler I, Berger W, Bertel O, Lüscher TF. Degenerative aortic valve stenosis, but not coronary disease, is associated with shorter telomere length in the elderly. *Arterioscler Thromb Vasc Biol.* 2006;26:e114–e117.
- Maubaret CG, Salpea KD, Jain A, Cooper JA, Hamsten A, Sanders J, Montgomery H, Neil A, Nair D, Humphries SE; HIFMECH consortium, Simon Broome Research Group. Telomeres are shorter in myocardial infarction patients compared to healthy subjects: correlation with environmental risk factors. *J Mol Med (Berl).* 2010;88:785–794.
- Panayiotou AG, Nicolaides AN, Griffin M, Tyllis T, Georgiou N, Bond D, Martin RM, Hoppensteadt D, Fareed J, Humphries SE. Leukocyte telomere length is associated with measures of subclinical atherosclerosis. *Atherosclerosis.* 2010;211:176–181.
- Salpea KD, Nicaud V, Tiret L, Talmud PJ, Humphries SE; EARS II group. The association of telomere length with paternal history of premature myocardial infarction in the European Atherosclerosis Research Study II. *J Mol Med (Berl).* 2008;86:815–824.
- Samani NJ, Boulby R, Butler R, Thompson JR, Goodall AH. Telomere shortening in atherosclerosis. *Lancet.* 2001;358:472–473.
- Aviv H, Khan MY, Skurnick J, Okuda K, Kimura M, Gardner J, Priolo L, Aviv A. Age dependent aneuploidy and telomere length of the human vascular endothelium. *Atherosclerosis.* 2001;159:281–287.
- Chang E, Harley CB. Telomere length and replicative aging in human vascular tissues. *Proc Natl Acad Sci U S A.* 1995;92:11190–11194.
- Okuda K, Khan MY, Skurnick J, Kimura M, Aviv H, Aviv A. Telomere attrition of the human abdominal aorta: relationships with age and atherosclerosis. *Atherosclerosis.* 2000;152:391–398.
- Matthews C, Gorenné I, Scott S, Figg N, Kirkpatrick P, Ritchie A, Goddard M, Bennett M. Vascular smooth muscle cells undergo telomere-based senescence in human atherosclerosis: effects of telomerase and oxidative stress. *Circ Res.* 2006;99:156–164.
- Ogami M, Ikura Y, Ohsawa M, Matsuo T, Kayo S, Yoshimi N, Hai E, Shirai N, Ehara S, Komatsu R, Naruko T, Ueda M. Telomere shortening in human coronary artery diseases. *Arterioscler Thromb Vasc Biol.* 2004;24:546–550.
- Dimri GP, Lee X, Basile G, Acosta M, Scott G, Roskelley C, Medrano EE, Linskens M, Rubelj I, Pereira-Smith O. A biomarker that identifies senescent human cells in culture and in aging skin *in vivo*. *Proc Natl Acad Sci U S A.* 1995;92:9363–9367.
- Hayashi T, Matsui-Hirai H, Miyazaki-Akita A, Fukatsu A, Funami J, Ding QF, Kamalanathan S, Hattori Y, Ignarro LJ, Iguchi A. Endothelial cellular senescence is inhibited by nitric oxide: implications in atherosclerosis associated with menopause and diabetes. *Proc Natl Acad Sci U S A.* 2006;103:17018–17023.
- Minamino T, Miyauchi H, Yoshida T, Ishida Y, Yoshida H, Komuro I. Endothelial cell senescence in human atherosclerosis: role of telomere in endothelial dysfunction. *Circulation.* 2002;105:1541–1544.
- Vasile E, Tomita Y, Brown LF, Kocher O, Dvorak HF. Differential expression of thymosin beta-10 by early passage and senescent vascular endothelium is modulated by VPF/VEGF: evidence for senescent endothelial cells *in vivo* at sites of atherosclerosis. *FASEB J.* 2001;15:458–466.
- Bürrig KF. The endothelium of advanced arteriosclerotic plaques in humans. *Arterioscler Thromb.* 1991;11:1678–1689.
- Repin VS, Dolgov VV, Zaikina OE, Novikov ID, Antonov AS, Nikolaeva MA, Smirnov VN. Heterogeneity of endothelium in human aorta. A quantitative analysis by scanning electron microscopy. *Atherosclerosis.* 1984;50:35–52.
- Satoh T, Sasatomi E, Yamasaki F, Ishida H, Wu L, Tokunaga O. Multinucleated variant endothelial cells (MVECs) of human aorta: expression of tumor suppressor gene p53 and relationship to atherosclerosis and aging. *Endothelium.* 1998;6:123–132.
- Tokunaga O, Satoh T, Yu S. Multinucleated variant endothelial cells (MVECs) have a greater capacity for LDL cholesterol uptake than typical mononuclear endothelial cells (TECs). *J Atheroscler Thromb.* 2002;9:35–41.
- Fenton M, Barker S, Kurz DJ, Erusalimsky JD. Cellular senescence after single and repeated balloon catheter denudations of rabbit carotid arteries. *Arterioscler Thromb Vasc Biol.* 2001;21:220–226.
- Breitschopf K, Zeiher AM, Dimmeler S. Pro-atherogenic factors induce telomerase inactivation in endothelial cells through an Akt-dependent mechanism. *FEBS Lett.* 2001;493:21–25.
- Imanishi T, Hano T, Nishio I. Angiotensin II accelerates endothelial progenitor cell senescence through induction of oxidative stress. *J Hypertens.* 2005;23:97–104.

32. Kurz DJ, Decary S, Hong Y, Trvier E, Akhmedov A, Erusalimsky JD. Chronic oxidative stress compromises telomere integrity and accelerates the onset of senescence in human endothelial cells. *J Cell Sci.* 2004;117(pt 11):2417–2426.
33. Imanishi T, Hano T, Nishio I. Estrogen reduces endothelial progenitor cell senescence through augmentation of telomerase activity. *J Hypertens.* 2005;23:1699–1706.
34. Kurz DJ, Hong Y, Trvier E, Huang HL, Decary S, Zang GH, Lüscher TF, Erusalimsky JD. Fibroblast growth factor-2, but not vascular endothelial growth factor, upregulates telomerase activity in human endothelial cells. *Arterioscler Thromb Vasc Biol.* 2003;23:748–754.
35. Vasa M, Breitschopf K, Zeiher AM, Dimmeler S. Nitric oxide activates telomerase and delays endothelial cell senescence. *Circ Res.* 2000;87:540–542.
36. Davies PF. Hemodynamic shear stress and the endothelium in cardiovascular pathophysiology. *Nat Clin Pract Cardiovasc Med.* 2009;6:16–26.
37. Nam D, Ni CW, Rezvan A, Suo J, Budzyn K, Llanos A, Harrison D, Giddens D, Jo H. Partial carotid ligation is a model of acutely induced disturbed flow, leading to rapid endothelial dysfunction and atherosclerosis. *Am J Physiol Heart Circ Physiol.* 2009;297:H1535–H1543.
38. Jaffe EA, Nachman RL, Becker CG, Minick CR. Culture of human endothelial cells derived from umbilical veins. Identification by morphologic and immunologic criteria. *J Clin Invest.* 1973;52:2745–2756.
39. Dardik A, Chen L, Frattini J, Asada H, Aziz F, Kudo FA, Sumpio BE. Differential effects of orbital and laminar shear stress on endothelial cells. *J Vasc Surg.* 2005;41:869–880.
40. Chakraborty A, Chakraborty S, Jala VR, Haribabu B, Sharp MK, Berson RE. Effects of biaxial oscillatory shear stress on endothelial cell proliferation and morphology. *Biotechnol Bioeng.* 2012;109:695–707.
41. Potter CM, Lundberg MH, Harrington LS, Warboys CM, Warner TD, Berson RE, Moshkov AV, Gorelik J, Weinberg PD, Mitchell JA. Role of shear stress in endothelial cell morphology and expression of cyclooxygenase isoforms. *Arterioscler Thromb Vasc Biol.* 2011;31:384–391.
42. Debacq-Chainiaux F, Erusalimsky JD, Campisi J, Toussaint O. Protocols to detect senescence-associated beta-galactosidase (SA-beta-gal) activity, a biomarker of senescent cells in culture and in vivo. *Nat Protoc.* 2009;4:1798–1806.
43. Chaudhury H, Zakkar M, Boyle J, Cuhmann S, van der Heiden K, Luong le A, Davis J, Platt A, Mason JC, Krams R, Haskard DO, Clark AR, Evans PC. c-Jun N-terminal kinase primes endothelial cells at atheroprone sites for apoptosis. *Arterioscler Thromb Vasc Biol.* 2010;30:546–553.
44. Foteinos G, Hu Y, Xiao Q, Metzler B, Xu Q. Rapid endothelial turnover in atherosclerosis-prone areas coincides with stem cell repair in apolipoprotein E-deficient mice. *Circulation.* 2008;117:1856–1863.
45. Lin K, Hsu PP, Chen BP, Yuan S, Usami S, Shyy JY, Li YS, Chien S. Molecular mechanism of endothelial growth arrest by laminar shear stress. *Proc Natl Acad Sci U S A.* 2000;97:9385–9389.
46. Heo KS, Lee H, Nigro P, Thomas T, Le NT, Chang E, McClain C, Reinhart-King CA, King MR, Berk BC, Fujiwara K, Woo CH, Abe J. PKC $\zeta$  mediates disturbed flow-induced endothelial apoptosis via p53 SUMOylation. *J Cell Biol.* 2011;193:867–884.
47. Kao CL, Chen LK, Chang YL, Yung MC, Hsu CC, Chen YC, Lo WL, Chen SJ, Ku HH, Hwang SJ. Resveratrol protects human endothelium from H(2)O(2)-induced oxidative stress and senescence via SirT1 activation. *J Atheroscler Thromb.* 2010;17:970–979.
48. Cheng C, Tempel D, van Haperen R, van der Baan A, Grosveld F, Daemen MJ, Krams R, de Crom R. Atherosclerotic lesion size and vulnerability are determined by patterns of fluid shear stress. *Circulation.* 2006;113:2744–2753.
49. Dai G, Kaazempur-Mofrad MR, Natarajan S, Zhang Y, Vaughn S, Blackman BR, Kamrn RD, García-Cardeña G, Gimbrone MA Jr. Distinct endothelial phenotypes evoked by arterial waveforms derived from atherosclerosis-susceptible and -resistant regions of human vasculature. *Proc Natl Acad Sci U S A.* 2004;101:14871–14876.
50. Ramkhelawon B, Vilar J, Rivas D, Mees B, de Crom R, Tedgui A, Lehoux S. Shear stress regulates angiotensin type 1 receptor expression in endothelial cells. *Circ Res.* 2009;105:869–875.
51. Akimoto S, Mitsumata M, Sasaguri T, Yoshida Y. Laminar shear stress inhibits vascular endothelial cell proliferation by inducing cyclin-dependent kinase inhibitor p21(Sdi1/Cip1/Waf1). *Circ Res.* 2000;86:185–190.
52. Mattiussi S, Turrini P, Testolin L, et al. p21(Waf1/Cip1/Sdi1) mediates shear stress-dependent antiapoptotic function. *Cardiovasc Res.* 2004;61:693–704.
53. Luo J, Nikolaev AY, Imai S, Chen D, Su F, Shiloh A, Guarente L, Gu W. Negative control of p53 by Sir2alpha promotes cell survival under stress. *Cell.* 2001;107:137–148.
54. Chen Z, Peng IC, Cui X, Li YS, Chien S, Shyy JY. Shear stress, SIRT1, and vascular homeostasis. *Proc Natl Acad Sci U S A.* 2010;107:10268–10273.
55. Zu Y, Liu L, Lee MY, Xu C, Liang Y, Man RY, Vanhoutte PM, Wang Y. SIRT1 promotes proliferation and prevents senescence through targeting LKB1 in primary porcine aortic endothelial cells. *Circ Res.* 2010;106:1384–1393.
56. Yeung F, Hoberg JE, Ramsey CS, Keller MD, Jones DR, Frye RA, Mayo MW. Modulation of NF-kappaB-dependent transcription and cell survival by the SIRT1 deacetylase. *EMBO J.* 2004;23:2369–2380.
57. Ota H, Eto M, Kano MR, Kahyo T, Setou M, Ogawa S, Iijima K, Akishita M, Ouchi Y. Induction of endothelial nitric oxide synthase, SIRT1, and catalase by statins inhibits endothelial senescence through the Akt pathway. *Arterioscler Thromb Vasc Biol.* 2010;30:2205–2211.
58. Gracia-Sancho J, Villarreal G Jr, Zhang Y, García-Cardeña G. Activation of SIRT1 by resveratrol induces KLF2 expression conferring an endothelial vasoprotective phenotype. *Cardiovasc Res.* 2010;85:514–519.
59. Dekker RJ, Boon RA, Rondaj MG, Kragt A, Volger OL, Elderkamp YW, Meijers JC, Voorberg J, Pannekoek H, Horrevoets AJ. KLF2 provokes a gene expression pattern that establishes functional quiescent differentiation of the endothelium. *Blood.* 2006;107:4354–4363.
60. Csiszar A, Smith K, Labinskyy N, Orosz Z, Rivera A, Ungvari Z. Resveratrol attenuates TNF-alpha-induced activation of coronary arterial endothelial cells: role of NF-kappaB inhibition. *Am J Physiol Heart Circ Physiol.* 2006;291:H1694–H1699.
61. Frankel EN, Waterhouse AL, Kinsella JE. Inhibition of human LDL oxidation by resveratrol. *Lancet.* 1993;341:1103–1104.
62. Wallerath T, Deckert G, Ternes T, Anderson H, Li H, Witte K, Förstermann U. Resveratrol, a polyphenolic phytoalexin present in red wine, enhances expression and activity of endothelial nitric oxide synthase. *Circulation.* 2002;106:1652–1658.
63. Santos AC, Veiga F, Ribeiro AJ. New delivery systems to improve the bioavailability of resveratrol. *Expert Opin Drug Deliv.* 2011;8:973–990.
64. Stein S, Schäfer N, Breitenstein A, Besler C, Winnik S, Lohmann C, Heinrich K, Brokopp CE, Handschin C, Landmesser U, Tanner FC, Lüscher TF, Matter CM. SIRT1 reduces endothelial activation without affecting vascular function in ApoE-/- mice. *Aging (Albany NY).* 2010;2:353–360.
65. Zhang QJ, Wang Z, Chen HZ, Zhou S, Zheng W, Liu G, Wei YS, Cai H, Liu DP, Liang CC. Endothelium-specific overexpression of class III deacetylase SIRT1 decreases atherosclerosis in apolipoprotein E-deficient mice. *Cardiovasc Res.* 2008;80:191–199.

## Significance

Although atherosclerosis is associated with systemic risk factors such as age, high cholesterol, and obesity, plaque formation occurs predominately at branches and bends that are exposed to disturbed patterns of blood flow. The molecular mechanisms that link disturbed flow-generated mechanical forces with arterial injury and disease are uncertain. In this article, we show for the first time that senescent endothelial cells accumulate at regions of disturbed flow in arteries. We conclude that the mechanism is related to cellular biomechanical responses because disturbed flow induced senescence in cultured endothelial cells via a p53-p21-dependent pathway. The study also demonstrates that flow-induced senescent endothelial cells are dysfunctional in terms of migration and inflammatory activation and thus may contribute to arterial disease processes. Finally, we demonstrated that pharmacological activation of sirtuin 1 can protect endothelial cells from flow-regulated senescence, thus paving the way for the development of novel treatments for arterial injury.

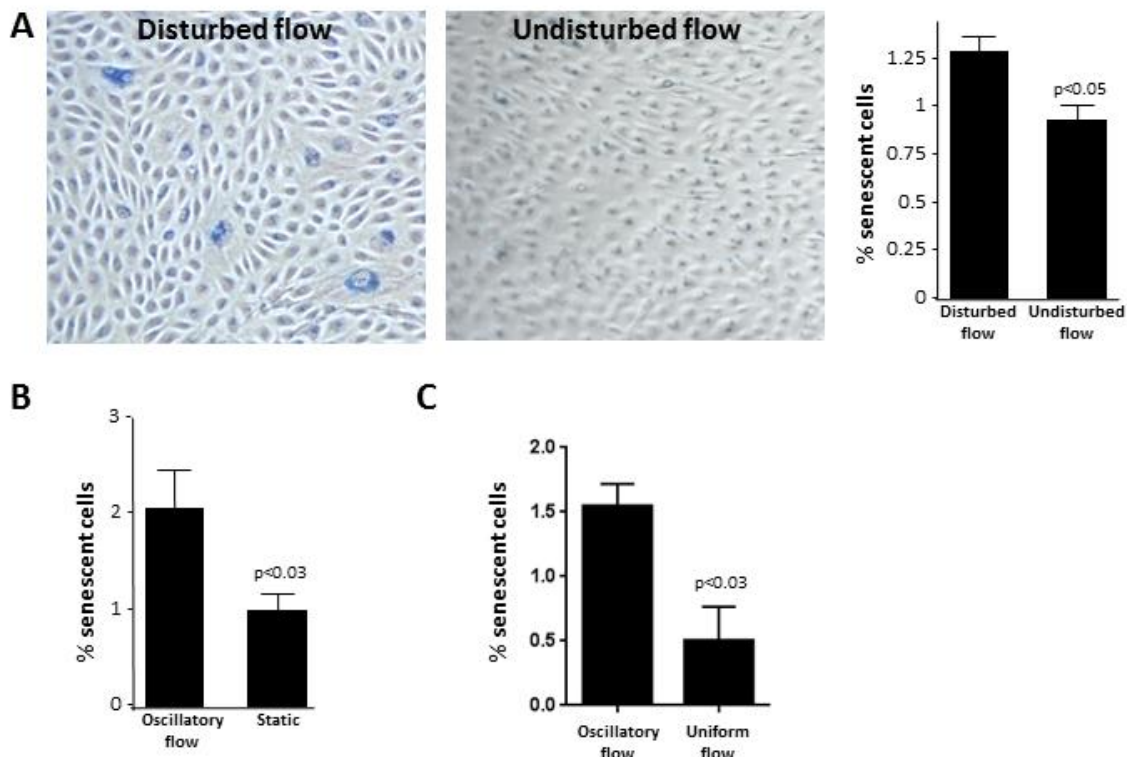
**Supplemental Figure I.**



**SA- $\beta$ -gal positive EC were identified at atherosusceptible sites.**

SA- $\beta$ -gal staining of porcine aortae ( $n=10$ ) was performed and analysed macroscopically (A) or following the Häutchen preparation (B).

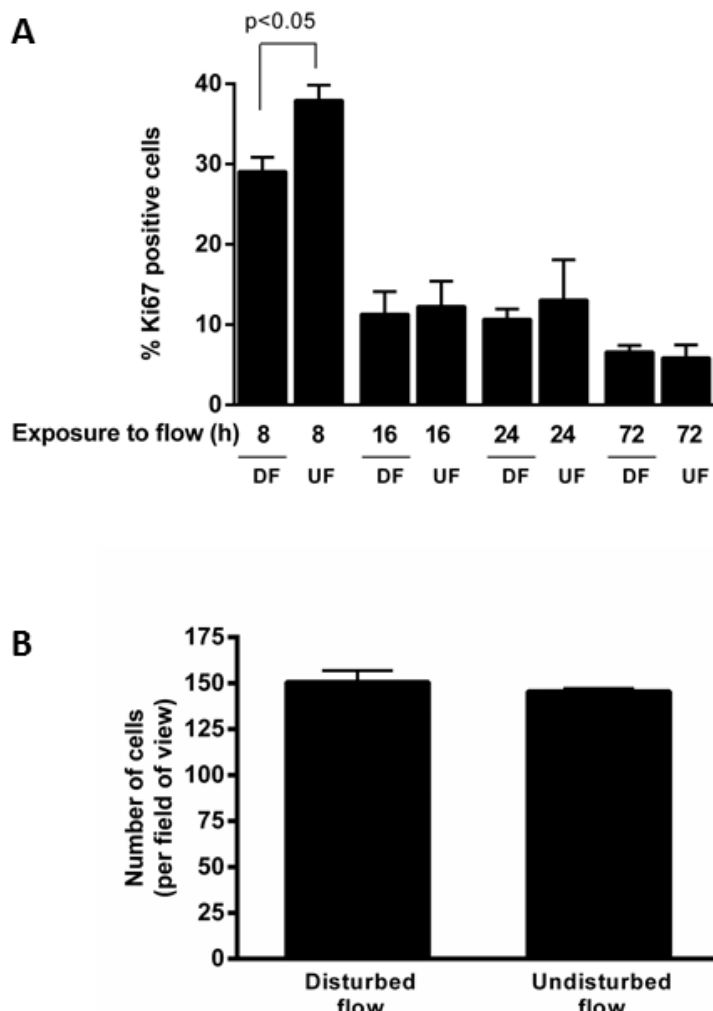
## Supplemental Figure II.



### Disturbed flow-induced senescence in cultured EC.

(A) PAEC were exposed to disturbed or undisturbed flow for 72h using the orbital system. (B, C) HUVEC were exposed to oscillatory ( $\pm$  5 dynes/cm $^2$ , 1 Hz) or unidirectional (13 dynes/cm $^2$ ; uniform) flow using a syringe-pump system, or remained under static conditions as a control. Endothelial senescence was assessed using the SA- $\beta$ -gal assay (A, B) and by quantifying large ( $> 100\mu\text{m}$  diameter) multinucleated cells (C). The percentage of senescent cells was calculated for each experimental condition. Data were pooled from at least three independent experiments and mean values are shown with standard errors.

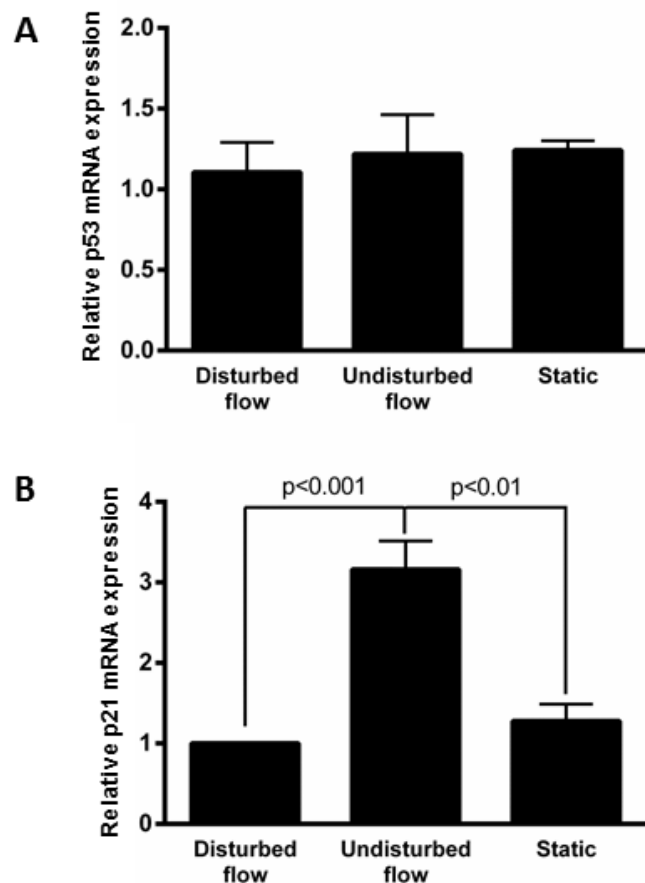
**Supplemental Figure III.**



**Disturbed flow-induced senescence was not associated with an increase in proliferation.**

(A) HUVEC were exposed to disturbed flow (DF) or undisturbed flow (UF) for 8-72h using the orbital system. Rates of proliferation were assessed periodically by immunostaining using antibodies that recognise the proliferation marker, Ki67. The percentage of Ki67-positive nuclei was determined in multiple fields of view per flow region in each experiment. (B) HUVEC were exposed to disturbed or undisturbed flow for 72 h and the number of cells per field of view was calculated (X40 magnification). Data were pooled from at least three independent experiments and mean values are shown with standard errors.

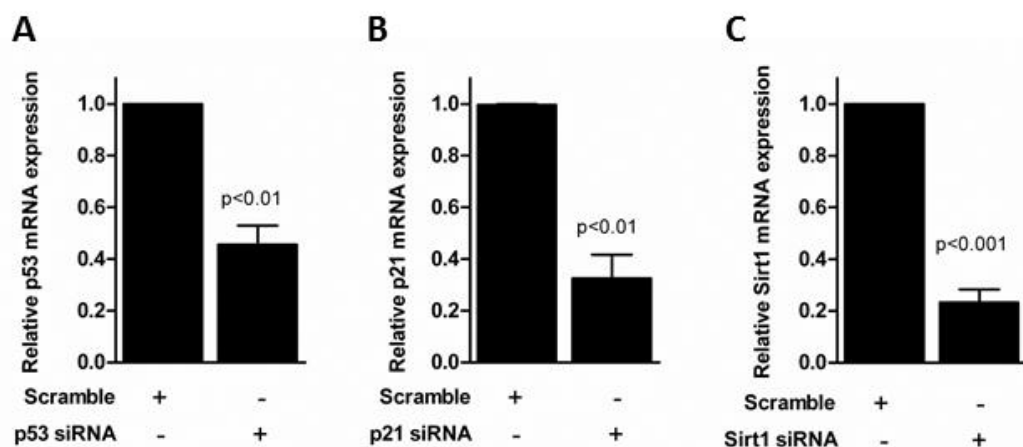
**Supplemental Figure IV.**



**Disturbed flow-induced senescence was not associated with elevated expression of p53 or p21 transcripts**

HUVEC were exposed to disturbed flow or undisturbed flow for 72 h or to static conditions as a control. Levels of p53 (A) or p21 (B) transcripts were quantified by qRT-PCR. Mean values pooled from three independent experiments are shown with standard errors.

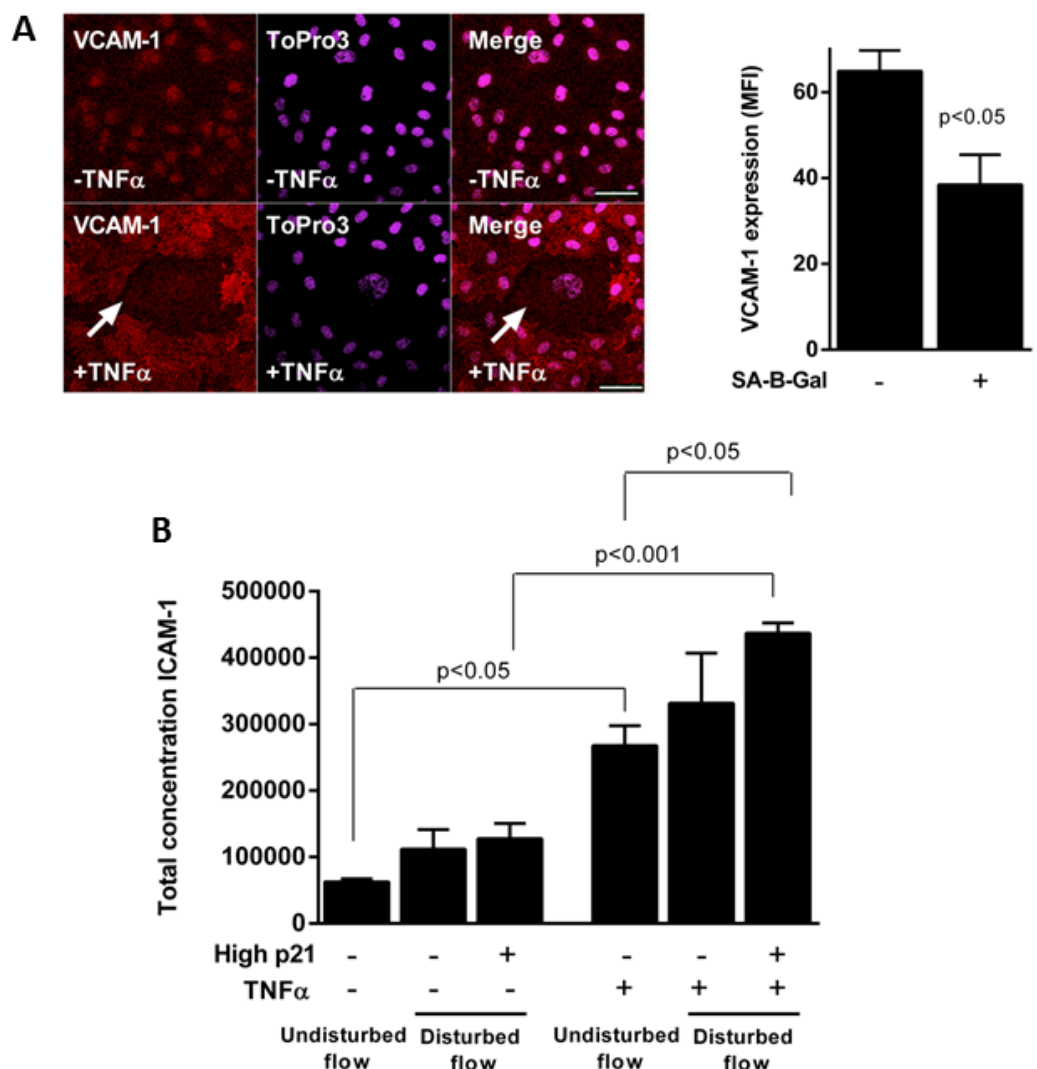
### Supplemental Figure V.



#### Validation of gene silencing following transfection with siRNA

The expression of (A) p53, (B) p21 and (C) sirtuin 1 (Sirt1) following 72 h exposure to flow was determined in HUVEC transfected with the corresponding siRNA relative to scramble-transfected controls by qRT-PCR. Mean values pooled from three independent experiments are shown with standard errors.

## Supplementary Figure VI.



### VCAM-1 expression is reduced in disturbed flow-induced senescent endothelial cells

(A) HUVEC exposed to disturbed flow for 72 h were exposed to TNF $\alpha$  (10 ng/ml for 4 h) or remained untreated prior to staining of VCAM-1 (red). Nuclei were stained with ToPro-3 (purple). Staining for SA- $\beta$ -gal was conducted in parallel and positive cells are marked by arrows. Representative images are shown (left). VCAM-1 mean fluorescence was calculated for SA- $\beta$ -gal-positive and SA- $\beta$ -gal negative cells and mean values are shown with standard deviations (right). Data were pooled from at least three independent experiments and mean values are shown with standard errors. (B) HUVEC exposed to disturbed flow for 72 h were exposed to TNF $\alpha$  (10 ng/ml for 18 h) or remained untreated prior to co-staining of ICAM-1 and p21. Staining for SA- $\beta$ -gal was conducted in parallel. Total expression levels of ICAM-1 (mean fluorescence  $\times$  cell area) were calculated for senescent (SA- $\beta$ -gal/ p21 positive) and non-senescent (SA- $\beta$ -gal/ p21 negative) cells and mean values are shown with standard errors. Data were pooled from three independent experiments.

## MATERIALS AND METHODS

**Animals** LDLR<sup>-/-</sup> mice were obtained from Jackson Laboratories and backcrossed onto the C57BL/6 background for ten generations (1). Mice were housed under specific-pathogen free conditions and studied according to UK Home Office Regulations and the UK Animals (Scientific Procedures) Act 1986. Mice were bred in-house and weaned at 4 weeks of age and maintained on a normal chow diet. All mice used in this study were female and experiments were performed using littermate controls in groups of at least 4 animals. Where indicated, normal chow diet was replaced at 10 weeks of age with a cholate-free high fat diet (Diet W) consisting of (w/w) cocoa butter (15%), cholesterol (0.25%), sucrose (40.5%), cornstarch (10%), corn oil (1%), cellulose (5.95%), casein (20%), 50% choline chloride (2%), methionine (0.2%) and mineral mixture (5.1%) for 2-6 weeks before sacrifice by CO<sub>2</sub> inhalation. Pig aortas from 4-6 month old animals (weight approx 80kg) were obtained immediately after slaughter from a local reputable abattoir.

**Reagents and antibodies** Human Sirt1 siRNA was from Santa Cruz. Human p53 and p21 siRNA, anti-p53 (7F5 rabbit polyclonal and 1C12 mouse monoclonal), and anti-p21 (12D1 rabbit polyclonal) were from Cell Signaling Technology. Non-targeting scrambled sequences were from Ambion. Anti-ICAM-1 (8.4A6 mouse monoclonal, (2)) and VCAM-1 (IG11 mouse monoclonal,(3)) were generously donated by Professor Dorian Haskard. Anti-Ki67 (rabbit polyclonal) was from Abcam. AlexaFluor 488- or 568-conjugated secondary antibodies and ToPro-3 were from Invitrogen. Aqueous mounting media was from Dako. qScript™ cDNA Supermix and PerfeCTa SYBR Green Supermix were from Quanta Biosciences. Griffonia lectin was from Vector Labs. Diet W was from Hope Farms (Woerden, Netherlands). All other reagents were from Sigma-Aldrich unless otherwise stated.

### ***En face* immunofluorescence staining**

After termination by CO<sub>2</sub> overdose, the animal was secured in a supine position. The abdomen was opened to the level of the diaphragm in a caudal to cranial manner before cutting through the sternum and removing the ribs. The vasculature was perfused with 20 ml sterile-filtered PBS injected by inserting a cannula (Venofix 23G; Medisave, UK) into the left ventricle. Perfusion fixation was carried out using 20ml 2% formalin (neutral buffer pH 7.0; VWR International) or 4% PFA (Sigma-Aldrich) in sterile/ filtered PBS which was introduced via the left ventricle. The aorta and the common carotid artery were removed and micro-dissected and adventitial fat thoroughly removed under a Zeiss Stereo dissecting microscope (Stemi-C, Zeiss; Germany). To assess the expression levels of specific proteins in ECs, the murine aortic arch was studied by *en face* immunofluorescence staining. ECs were permeabilised using 0.5% Triton X-100, and then blocked by incubating with 20% goat serum (corresponding to the species used to raise secondary antibodies) overnight at room temperature. After washing with PBS (3 x 5 min using PBS), the tissue was incubated with unconjugated primary antibodies overnight at 4 °C. The tissue was then washed with PBS and incubated with appropriate secondary antibodies for 2-3 h at room temperature followed by incubation with anti-CD31 antibodies (directly conjugated to Alexafluor 488) for 72 h at 4°C. After washing (3 x 5 min using PBS), the tissue was incubated with ToPro-3 for 30 min to counterstain nuclei. To control for specific binding, tissue was incubated with isotype-matched irrelevant IgG antibodies and appropriate fluorescent secondary antibodies, or with secondary antibodies alone. The ascending aorta and arch were opened and mounted using Fluoromount-G mounting medium (eBioscience, Hatfield, UK) with the endothelium facing the coverslip. Images of the endothelial cell monolayer were obtained using an inverted laser-scanning confocal microscopy (LSM 510 Meta inverted; Zeiss, Oberkochen, Germany). Tissue incubated in secondary antibody only was used to control for background staining or autofluorescence and to optimise the confocal settings. Protected (outer curvature) and susceptible (inner curvature) regions of the ascending aorta were located using anatomical landmarks described by Iiyama and colleagues<sup>3</sup>. It has been established that ECs at the athero-protected site are aligned whereas EC at the athero-susceptible region are more

irregular and polygonal in morphology. Therefore, the morphology of ECs was also used to confirm imaging at the correct region. For each animal, three or four images were obtained from each atheroprotected and atherosusceptible region. The proportion of positive cells at each site was quantified by analysis of multiple fields of view from atherosusceptible or atheroprotected sites, and expressed as percentage positivity. Specialised Zeiss LSM Meta software was used to measure the mean fluorescent intensity (MFI) in multiple cells (>50 cells) in multiple fields of view and mean values were calculated after pooling data.

**Endothelial cell isolation and culture** HUVEC and PAEC were isolated using collagenase digestion as described previously (4). HUVEC were cultured on 1% gelatin and maintained in M199 growth medium supplemented with foetal bovine serum (20%), L-glutamine (4 mmol/L), endothelial cell growth supplement (30 µg/ml), penicillin (100 U/ml), streptomycin (100 µg/ml) and heparin (10 IU/ml).

### **Application of flow**

**Orbital shaker method.** EC were seeded at passage 3-5 onto fibronectin-coated 6-well plates. Where experiments required immunostaining, EC were seeded onto 34mm glass cover slips stuck to the bottom of the well. Once monolayers were confluent (after 24-48hrs), the 6-well plates were placed onto an orbital rotating platform (Grant Instruments) housed inside the incubator and cultured for a further 72 h. The radius of orbit of the orbital shaker was 10mm and the rotation rate was set to 210rpm which caused swirling of the culture medium over the cell surface. The behaviour of fluid in a cylindrical cell culture dish exposed to orbital motion was modelled using commercial computational fluid dynamics (CFD) software (Fluent 6.2, ANSYS). A 3D cylinder with the same dimensions of the culture well was created in the pre-processor Gambit (ANSYS, Inc.) and then a mesh of approximately 300,000 hexahedral elements was applied to the volume. The rotation of the well was described using a dynamic grid that moved through space, where orbital radius, orbital speed, and centre of orbit, were assigned by a user defined function. The movement of fluid due to orbital motion represents a free surface flow at the liquid-air interface that was established by the volume of fluid (VOF) model. A transient solution was required since the location of the fluid domain is changing with time and the solution took several rotations to achieve steady state. Wall shear stress magnitude and direction at the base of the well were derived from the computed flow field.

### **Syringe pump methods.**

Confluent monolayers of HUVEC (passage 3-5) were seeded onto fibronectin-coated µ-slide chambers (Ibidi GmbH, Germany) and used at confluence. Flow was generated using an in-house syringe pump system, in which a 20ml syringe was inserted into a computer-controlled syringe pump (Kent Scientific) that was programmed to produce an oscillatory flow of +/- 9 ml/min at 1 Hz. This resulted in a wall shear stress of +/- 5 dynes/cm<sup>2</sup> in an Ibidi flow chamber (flow chamber height = 0.6mm, flow chamber width = 5mm) that was connected to the syringe via a three-way tap. A second 20ml syringe containing approximately 10ml of culture medium and 5ml of air was attached to the Ibidi flow chamber at its outlet. Air was included in the syringe at the outlet to ensure that only minimal pressure variations were caused by the oscillatory flow. Alternatively, oscillatory flow ( $\pm 5$  dyne/cm<sup>2</sup> at 2 Hz) or high unidirectional flow (13 dynes/cm<sup>2</sup>) was applied using the ibidi® pump system (ibidi GmbH, Germany). Complete cell growth medium was perfused in the flow system and the pump system was maintained at 37°C and 5% CO<sub>2</sub> in a humidified incubator for up to 48 h. Time-lapse imaging of cells under flow was acquired using the Rolera™ Bolt CMOS camera attached to the Nikon TE-300 inverted microscope (x10 objective lens).

**Senescence-associated β-galactosidase assay** Senescent EC were identified by a chromogenic assay of SA-β-gal activity at pH 6.0 (5). HUVEC were fixed for 15 min with glutaraldehyde (0.5%) and then washed twice with PBS containing MgCl<sub>2</sub> (1 mmol/L) adjusted to pH 6.0. Monolayers were then incubated for 2 - 4 h at 37°C with SA-β-gal

staining solution: 5-bromo-4-chloro-3-indoyl  $\beta$ -D-galactopyranoside (X-Gal; 1mg/ml), potassium ferrocyanide (5 mmol/L) and potassium ferricyanide (5 mmol/L) in PBS (pH 6.0.) X-Gal was from a stock solution (20mg/ml) in N,N-dimethylformamide. Following incubation, monolayers were washed twice with PBS and viewed under phase contrast using an Olympus BX50 microscope. EC were identified as being senescent by the presence of an insoluble blue reaction product. The percentage of SA- $\beta$ -gal positive cells was calculated per field of view with multiple fields of view examined per well.

For detection of SA- $\beta$ -gal activity in pig aortas, vessels were fixed with formaldehyde (2%) plus glutaraldehyde (0.25%) for 10 min. The aortas were washed with PBS (pH 6.0) and incubated with X-Gal staining solution as described above for 2-24 h. For detection of SA- $\beta$ -gal activity in mouse aortas the vasculature was perfused *in situ*, immediately after sacrifice, with cold PBS via the left ventricle and then fixed with paraformaldehyde (4 %) for 5 min. Aortas were removed and dissected longitudinally along the inner curvature to the iliac bifurcation in cold PBS (pH 6.0). A small incision was made along the outer curvature from the aortic root to the brachiocephalic artery allowing the aorta to be pinned out flat. Aortas were incubated with X-Gal staining solution as described above for 2-16 h and examined en face.

**Häutchen Preparations** To assess whether SA- $\beta$ -gal activity was localized to EC of the aorta, Häutchen preparations were made following incubation with X-Gal staining solution. Vessels were dehydrated by immersion in a graded series of ethanol (30% to 100%) and allowed to dry. Once the ethanol had evaporated aortas were pressed firmly, lumen-side down, onto a piece of double-sided sticky tape adhered to a microscope slide. Samples were rehydrated by immersion in glycerol (10%) before the tissue was carefully peeled away leaving only the endothelium on the tape. Preparations were air-dried before phase contrast imaging using an Olympus BX50 microscope.

**Gene silencing** RNA interference was performed using siRNA sequences specific for human target genes Non-targeting scrambled sequences were used as a control. Immediately prior to seeding into 6-well plates HUVEC were transfected with siRNA (100 nmol/L final concentration) by electroporation (Neon™ Transfection System, Invitrogen) according to the manufacturer's instructions. Transfected cells were cultured for 24 h before exposing to flow for 72 h.

**Quantitative RT-PCR** Total RNA was prepared from HUVEC using a QIAGEN RNeasy Kit according to the manufacturer's instructions. cDNA (0.5  $\mu$ g) was prepared using qScript™ cDNA Supermix according to the manufacturer's instructions. Transcript levels were determined by qRT-PCR using gene-specific primers (p53, sense GCCCCCCAGGGAGCACTA, antisense GGGAGAGGAGCTGGTGTG; p21, sense GATGTCCGTCAGAACCCATG, antisense TTAGGGCTCCTCTGGAGA; Sirt1, sense CGTCTTATCCTCTAGTTCTGTG, antisense ATCTCCATCAGTCCCAAATCC; GAPDH, sense CAAGGTCTATCCATGACAACTTG, antisense GGGCCATCCACAGTCTTCTG), PerfeCTa SYBR Green Supermix and an CFX96™ Real-Time PCR Detection System (Bio-Rad). Reactions were incubated at 95°C for 3 min followed by 40 cycles of 95°C for 15 seconds, 55-65°C for 30-45 seconds and 68-72°C for 30 seconds. All reactions were performed in triplicate and quantified as described previously using the  $\Delta\Delta Ct$  method and GAPDH as a house-keeping gene (6).

**Immunofluorescence staining** The expression levels of proteins were assessed by immunostaining using specific anti-human antibodies followed by laser-scanning confocal microscopy. HUVEC were fixed with formaldehyde (4%) and permeabilised with Triton X-100 (0.1%). Following blocking with goat serum for 1 h monolayers were incubated with primary antibodies against p53, p21, ICAM-1, VCAM-1 or Ki67 followed by the relevant AlexaFluor 488- or 568-conjugated secondary antibodies. Nuclei were counter-stained using ToPro-3.

Cover slips were mounted onto microscope slides using aqueous mounting media and imaged using a Zeiss LSM 510 META laser-scanning confocal microscope. The mean fluorescence intensities (MFI) for multiple cells in multiple fields of view were determined using Zeiss LSM 510 META image analysis software using identical laser power and detector gain settings. Isotype controls or omission of the primary antibody was used to control for non-specific staining.

The activity of SA- $\beta$ -gal was assessed in mouse aortas using a fluorescent analogue of X-Gal, dodecanoylaminofluorescein di- $\beta$ -galactopyranoside ( $C_{12}$ FDG). Following sacrifice the vasculature was perfused *in situ* with cold PBS and fixed with paraformaldehyde (4 %) for 30 min. Aortas were removed and stored in PBS (pH 6.0) for 18 h followed by incubation with  $C_{12}$ FDG (2 mmol/L) for 3 h at 37°C. Aortas were then incubated with rhodamine-conjugated Griffonia lectin to identify endothelial cells followed by ToPro3 to identify nuclei. The aortic arch was dissected, mounted and imaged en face using laser-scanning confocal microscopy as previously described (7). The MFI was determined for multiple fields of view within areas of disturbed and undisturbed flow from each animal and expressed as relative increase in MFI.

**Scratch-Migration Assay** Scratch wounds were created on confluent monolayers using a rubber cell scraper (1 mm width) and migration of EC into the wounded area visualised using time-lapse confocal microscopy (Zeiss LSM 510 META). Images were captured at 15 min intervals for 18 h after wounding. The migration velocity, direction and distance of individual cells was assessed using ImageJ Software Version 1.43 (National Institutes of Health) with manual tracking (Institut Curie) and chemotaxis (Ibidi) plug-ins enabled. In order to track the migration of senescent EC, monolayers were assayed for SA- $\beta$ -gal activity as described above following live-cell imaging and the regions of interest identified by phase-contrast microscopy.

**Statistics** Data are expressed as mean  $\pm$  SEM. Statistical comparisons were made by two-tailed unpaired Students t-test unless otherwise stated. P values of  $<0.05$  were considered statistically significant.

## REFERENCES

1. Bhatia VK, Yun S, Leung V, Grimsditch DC, Benson GM, Botto MB, Boyle JJ, Haskard DO. Complement c1q reduces early atherosclerosis in low-density lipoprotein receptor-deficient mice. *Am J Pathol*. 2007;170:416-426.
2. Wellicome SM, Thornhill MH, Pitzalis C, Thomas DS, Lanchbury JS, Panayi GS, Haskard DO. A monoclonal antibody that detects a novel antigen on endothelial cells that is induced by tumor necrosis factor, il-1, or lipopolysaccharide. *The Journal of Immunology*. 1990;144:2558-2565.
3. Wellicome SM, Kapahi P, Mason JC, Lebranchu Y, Yarwood H, Haskard DO. Detection of a circulating form of vascular cell adhesion molecule-1: Raised levels in rheumatoid arthritis and systemic lupus erythematosus. *Clin Exp Immunol*. 1993;92:412-418
4. Jaffe EA, Nachman RL, Becker CG, Minick CR. Culture of human endothelial cells derived from umbilical veins. Identification by morphologic and immunologic criteria. *The Journal of Clinical Investigation*. 1973;52:2745-2756.
5. Debacq-Chainiaux F, Erusalimsky JD, Campisi J, Toussaint O. Protocols to detect senescence-associated beta-galactosidase (sa-[beta]gal) activity, a biomarker of senescent cells in culture and in vivo. *Nat. Protocols*. 2009;4:1798-1806.
6. Partridge J, Carlsen H, Enesa K, Chaudhury H, Zakkar M, Luong L, Kinderlerer A, Johns M, Blomhoff R, Mason JC, Haskard DO, Evans PC. Laminar shear stress acts as a switch to regulate divergent functions of nf-kappab in endothelial cells. *FASEB J*. 2007;21:3553-3561.
7. Iiyama K, Hajra L, Iiyama M, Li H, DiChiara M, Medoff BD, Cybulsky MI. Patterns of vascular cell adhesion molecule-1 and intercellular adhesion molecule-1 expression in rabbit and mouse atherosclerotic lesions and at sites predisposed to lesion formation. *Circulation Research*. 1999;85:199-207.